*J. Fluid Mech.* (2008), *vol.* 596, *pp.* 103–132. © 2008 Cambridge University Press
doi:10.1017/S0022112007009330 Printed in the United Kingdom


# On the spatial length scales of scalar dissipation in turbulent jet flames

P. VAISHNAVI[1], A. KRONENBURG[1]† AND C. PANTANO[2]

[1]Department of Mechanical Engineering, Imperial College, London SW7 2AZ, UK

[2]Department of Mechanical Science and Engineering, University of Illinois at Urbana-Champaign, Urbana, IL 61801, USA

(Received 3 November 2006 and in revised form 25 September 2007)

Spatial length scales of the rate of dissipation, $\chi$, of fluctuations of a conserved scalar, $Z$, are inferred numerically using a DNS database of a turbulent planar jet flame. The Taylor-scale Reynolds numbers lie in the range of 38 to 58 along the centreline of the simulated jet flame. Three different methods are used to study the spatial length scales associated with $\chi$. First, analysis of the one-dimensional dissipation spectra shows an expected $Re_\delta{}^{-3/4}$ (Kolmogorov) scaling with the outer-scale Reynolds number, $Re_\delta$. Secondly, thin sheet-like three-dimensional scalar dissipation structures have been investigated directly. Such structures were identified within the computational domain using level-sets of the $\chi$-field, and their thicknesses were subsequently computed. The study shows, in accordance with experimental studies, that the captured dissipation-layer thickness also shows a Kolmogorov scaling with $Re_\delta$. Finally, spatial filters of varying widths were applied to the instantaneous $Z$ field in order to model the averaging effect that takes place with some experimental measurement techniques. The filtered scalar dissipation rate was then calculated from the filtered scalar field. The peaks in the instantaneous filtered $\chi$-profiles are observed to decrease exponentially with increasing filter width, yielding estimates of the true value of $\chi$. Unlike the dissipation length scales obtained from the spectral analysis and the level-set method, the length-scale estimates from the spatial-filtering method are found to be proportional to $Re_\delta{}^{-1}$. This is consistent with the small-scale intermittency of $\chi$ which cannot be captured by techniques that just resolve the conventional Batchelor/Obukhov–Corrsin scale. These results have implications when considering resolution requirements for measuring scalar dissipation length scales in experimental flows.

## 1. Introduction

The rate of scalar dissipation, also referred to as the scalar dissipation for short, is regarded as a central concept in the theory of laminar and turbulent non-premixed combustion (Bilger 1980, 2004; Williams 1985; Pitts, Richards & Levenson 1999; Peters 2000). Mathematically, the instantaneous scalar dissipation is defined as

$$\chi = 2D\nabla Z' \cdot \nabla Z' \simeq 2D\nabla Z \cdot \nabla Z, \tag{1.1}$$

where $D$ is an appropriate molecular diffusion coefficient, $Z(\boldsymbol{x}, t)$ is a conserved scalar field known as the mixture fraction that varies in space, $\boldsymbol{x}$, and time, $t$, and which has

† Author to whom correspondence shoud be addressed: a.kronenburg@imperial.ac.uk

the value of zero in the unmixed oxidizer stream and unity in the unmixed stream containing the fuel. The quantity $Z'$ denotes the deviation of $Z$ from the mean or average value. According to (1.1), $\chi$ is directly proportional to the square of the magnitude of the scalar gradient, and it can be shown that the average of $\chi$ quantifies the rate of molecular mixing in a flow field, or equivalently, the rate at which the average variance of scalar fluctuations, $Z'^2$, is destroyed (Tennekes & Lumley 1974). While there is good evidence to suggest that the statistics of $\chi$ have some properties of a near-universal nature (Monin & Yaglom 1971; Nelkin 1994; Sreenivasan & Antonia 1997; Wang, Chen & Brasseur 1999) that can be applied to many mixing environments, including the ocean, the atmosphere and internal flows of engineering importance, the departures from the universal behaviour (specifically for the inertial-subrange) have also been well documented (Frisch 1991; Sreenivasan & Stolovitzky 1996; Noullez *et al.* 1997). Frisch (1995) gives a detailed review of these aspects in the theory of small-scale turbulence. In this paper, we concentrate primarily on results pertaining to reacting flows, for which turbulent scalar mixing is less well-studied in spite of its crucial role in such flows (Bilger 1980).

Understanding the statistical properties of a random quantity such as $\chi$ is the starting point for developing improved models for mixing and for non-premixed combustion. Experimentally, it is observed that the statistical behaviour of $\chi$ is similar to that of the instantaneous turbulence dissipation, $\epsilon$, in terms of their strong intermittency. In other words, a frequent occurrence of instantaneous values much larger than the mean is observed. However, the frequency and magnitudes of the fluctuations in $\chi$ are characteristically larger than those in $\epsilon$. Nonetheless, both variables show a skewed PDF that has a large tail.

It follows from the studies of Batchelor & Townsend (1949), Grant, Stewart & Moilliet (1962) and Meneveau & Sreenivasan (1991) that the average value of $\epsilon(\boldsymbol{x}, t)$ is not representative of the full viscous dissipation characteristics, and the reader is referred to the reviews by Sreenivasan (2004) and Schumacher, Sreenivasan & Yeung (2005). Attempts to incorporate the high-variability properties of $\epsilon$ into a turbulence theory led to the well-known work of Kolmogorov (1962). In this respect, Oboukhov (1949) and Corrsin (1951) were the first to assume that many aspects of turbulent mixing are similar to turbulence itself and predicted the scaling of the inertial subranges of structure functions and spectra.

Experimental measurement of the scalar dissipation entails the difficult task of obtaining the instantaneous spatial derivative (in at least one dimension) of the mixture fraction with sufficient resolution that these frequent large-magnitude excursions are not overlooked (Gibson 1991). The experimental study by Dahm & Southerland (1997) gives an assessment of the accuracy of Taylor's hypothesis in approximating the magnitude of the scalar dissipation rate from such one- or two-dimensional spatio-temporal measurements of the scalar gradients. Furthermore, the study quantifies the extent of the departure from the true magnitudes using such measurements and gives a generalized analytical framework to maximize the correlation between the measured and true dissipation rates. There have been many other recent attempts (experimental and numerical studies) to quantify scalar dissipation in turbulent axisymmetric and planar jets, such as those by Dahm, Southerland & Buch (1991), Buch & Dahm (1996, 1998), Dahm & Southerland (1999), Pitts *et al.* (1999), Tsurikov & Clemens (2002), Su & Clemens (2003) and Barlow & Karpetis (2005*b*). An additional difficulty encountered in reacting flows is that the mixture fraction itself does not exist on its own as part of the experimental flow. It is generally derived from the composition of the mixture (Bilger,

Stårner & Kee 1990). This requires simultaneous measurements of multiple species concentrations in a high-temperature environment as a prelude to obtaining the scalar dissipation. This interest is motivated by a desire to characterize this fundamental turbulence property and to model its behaviour owing to its key role in mixture-fraction-based models for turbulent non-premixed or partially premixed combustion.

As most of the contributions to the statistics for scalar dissipation come from the finest mixing scales of turbulence (see the reviews by Bilger 2004; Sreenivasan 2004), the problem of reliable measurements of this quantity is further complicated by the trade-off between higher resolution, corresponding to smaller experimental probe-width, and greater signal-to-noise ratio. Thus, analysis of resolution requirements of the scalar dissipation is of paramount importance. Owing to these inherent experimental diagnostic limitations, studies such as Buch & Dahm (1996, 1998) Pitts *et al.* (1999) and Su & Clemens (2003) have attempted to characterize the scalar dissipation dynamics in non-reacting flows and extend the findings to turbulent combustion. In this paper, we discuss results obtained by analysing direct numerical simulation (DNS) data of a very well resolved mixture fraction field (Pantano 2004) according to several criteria. Reynolds-number scaling and one-point statistics of the scalar dissipation are presented and discussed.

## 2. Scalar dissipation length scales

### 2.1. *Average and instantaneous dissipation length scales*

The Kolmogorov length scale of turbulence is defined as

$$\eta = \left( \frac{\nu^3}{\langle \epsilon \rangle} \right)^{1/4}, \tag{2.1}$$

where $\langle \epsilon \rangle$ denotes the mean of the turbulence kinetic energy dissipation rate, $\epsilon(\boldsymbol{x}, t)$, and $\nu$ is the kinematic viscosity. The mechanism of formation of turbulent fluid-elements with a characteristic thickness of $\eta$ can be explained in terms of the vorticity transport equation, which describes the evolution of the vorticity field subject to the balance between vortex-stretching due to the mean strain-rate field (resulting in an elongation and thinning of the vortex-tube structures) and the reconnection effects induced by viscous-diffusion. The result is a vortex tube with $O(\eta)$ thickness, characterizing the length scale at which the viscous dissipation of turbulent kinetic energy predominates.

The average dissipation length scale $\eta$ is undoubtedly important from a theoretical and practical standpoint. However, owing to the attested departure from Gaussianity in the dissipation range (Monin & Yaglom 1971), it is unable to fully characterize the distribution of dissipation scales in turbulent flow. This multiplicity of dissipation length scales is characteristic of the small-scale intermittency, and its physical explanation involves the addition of a new feature to the traditional eddy-cascade picture of turbulence by Kolmogorov (1941). She, Jackson & Orszag (1990) and She (1991) describe the canonical picture of turbulence as consisting of a hierarchy of small-scale coherent structures in addition to the known random eddy-cascade with near-Gaussian statistics. These coherent structures are local and intermittent and, thus, show strongly non-Gaussian statistics. The aforesaid mechanism of formation of coherent vortex structures, based on the strain–diffusion balance, is supplemented in the revised picture. She *et al.* (1990) describe the coherent vortex structures as being subjected to an additional strain field caused by the vortex structures themselves in the

event of large vorticity magnitudes. To account for this *self-stretching* component of the strain rate, the strain-rate tensor is subdivided into the self-stretching and mean-strain components. The former component becomes dominant at high vorticity (or, equivalently, large velocity-gradient) magnitudes. The balance between the dominant self-stretching component of strain rate and the viscous diffusion leads to the formation of structures with sub-Kolmogorov thicknesses and results in the wide dissipation length-scale distribution characteristic of intermittency. It is important to note here that the descriptions of turbulence intermittency in Kolmogorov (1962) and related studies presume the dissipation-scale statistics as lognormal-like. Unlike She *et al.* (1990) and She (1991), these descriptions do not fully explain/model the turbulence dynamics underlying such statistics.

For the reasons described above and in some circumstances, it becomes useful to define a local, instantaneous, viscous dissipation length scale, called the local Kolmogorov scale by Schumacher *et al.* (2005) and denoted here by $\eta'$. The concept of a locally defined, fluctuating dissipation length-scale is not new, and has also been put forth in the multifractal analysis of the small-scale turbulence structure by Frisch & Vergassola (1991). This local quantity follows from (2.1) according to the same dimensional arguments as used to define $\eta$, giving $\eta'(\boldsymbol{x}, t) \sim (\nu^3/\epsilon(\boldsymbol{x}, t))^{1/4}$. Since $\nu$ is not expected to have very intermittent statistics, it largely depends on some smooth function of the temperature, the majority of the variability of $\eta'$ results from the statistics of $\epsilon$. The abundance of local values of $\epsilon$ that are much larger than $\langle\epsilon\rangle$ (owing to its intermittent distribution) gives rise to a significant range of instantaneous dissipation length scales smaller than $\eta$. Accurately measuring the probability distribution function (or PDF) of $\epsilon$ requires that the minimum measuring scale, $\eta_{min} \sim \left(\nu^3/\epsilon_{max}\right)^{1/4}$, be such that the probability that $\epsilon > \epsilon_{max}$ is very small, say 1% (Sreenivasan 2004).

The same argument of small-scale intermittency can be extended to turbulent mixing dynamics, as explained in Sreenivasan (1991, 2004) and Bilger (2004), to hypothesize the existence and significance of local scalar dissipation length scales, or $\eta_Z = \eta Sc^{-3/4}$, where $\eta_Z$ denotes the Obukhov-Corrsin scale. This expression is valid for Schmidt numbers, $Sc$, smaller than one, and $Sc$ is defined as $Sc = \nu/D$ (Tennekes & Lumley 1974). For large Schmidt numbers, $Sc \geqslant 1$, the corresponding balance of turbulent stretching and molecular diffusion leads to the Batchelor (1959) scale, defined as $\eta_Z = \eta Sc^{-1/2}$. While the definition of the Batchelor scale is strictly valid for Schmidt numbers greater than or equal to unity (Buch & Dahm 1998), the label is commonly used to imply the finest mixing scale in the turbulence and combustion literature. Hereinafter, for the sake of convenience, all references to the Batchelor scale will imply the finest mixing-length scale in the broadest sense, whereas the symbol $\eta_Z$ will be used to denote the specific Schmidt number scaling for the present case of $Sc = 0.7$. It should be noted that the difference in value between the Batchelor and Obukhov–Corrsin scales is negligible for Schmidt numbers of order unity.

### 2.2. *Categorization of the measurement methods*

The experimental or numerical measurement of spatial scales associated with scalar dissipation can be broadly categorized into approaches that involve either the computation of two-point spatial correlations of scalar fluctuations (scalar spectra), or the determination of the spatial distribution of the scalar dissipation using scalar gradients.

The method involving scalar spectra uses the standard eddy-cascade theory of turbulence to arrive at estimates for the Batchelor length scale and is described in § 4. On the other hand, information about the spatial distribution of $\chi$ can, in turn, be acquired through two independent approaches used in the literature that either compute the spatial variation of $\chi$ by plotting its iso-contours or level sets at various fractional values of the local peak, keeping the grid-size fixed, or that model the decay of the local peak values in the $\chi$-profiles for incremental increases in the effective spatial discretization (or filter width) of the sampling volume.

The former level-set (fixed filter-width) approach has been used in various numerical and experimental studies, such as those by Buch & Dahm (1996, 1998), Kushnir, Schumacher & Brandt (2006*b*), Su & Clemens (2003) and Tsurikov & Clemens (2002), to investigate the thin planar three-dimensional scalar-dissipation structures and ascertain their thicknesses. The thicknesses thus computed are characterized as the spatial scales associated with scalar dissipation. The application of this approach to the present study is detailed in § 5. Other experimental studies by Barlow & Karpetis (2005*a*, *b*) estimate $\chi$ using the latter spatial-filtering approach. As described further in § 6, this method in particular seems better suited for characterizing the small-scale intermittency of the scalar-dissipation process.

The main motivation of the present study is to attempt a numerical implementation of all of the above-mentioned approaches to characterize the spatial length scales of the scalar dissipation in terms of easily measurable large-scale properties of the flow such as the outer-scale turbulent Reynolds number. The following section outlines the key features of the analysed DNS database. A detailed description of the aforesaid approaches, the limitations involved in their implementation to the DNS database and the discussion of (and comparison between) the results are detailed in § 4 and onwards.

## 3. The numerical experiment

### 3.1. *Choice of the DNS database*

Traditionally, simulations involving the solution of the scalar advection diffusion equation with the Navier–Stokes equations have resolved no more than the Batchelor scale. Experiments in non-reacting flows by Buch & Dahm (1996, 1998), Pitts *et al.* (1999) and Su & Clemens (2003) among others have also suggested that accurate measurements of the scalar dissipation rate require a spatial resolution comparable to (or even smaller than) the Batchelor scale, using scaling laws and self-similarity arguments. However, as Barlow & Karpetis (2005*b*) suggest, applicability of these scaling relationships to estimating the Batchelor scale in laboratory-scale flames is unclear. Such estimates are hinged on the assumption of self-similarity of the flow that is valid only far downstream, if present at all in common flame geometries (Sreenivasan 2004). Furthermore, owing to the reasons described in the preceding section, the intermittent character of the scalar dissipation process introduces additional constraints on its spatial resolution and the Batchelor-scale estimate is no longer enough for moments higher than the mean. Hence, various reviews by Bilger (2004), Sreenivasan (2004), Barlow & Karpetis (2005*b*), and Schumacher *et al.* (2005) concur that published $\chi$-measurements from experiments or simulations of turbulent jet flames can frequently have questionable spatial resolution, especially at high Reynolds numbers.

Many recent well-resolved simulations of turbulent scalar mixing in the literature are in the low (Yeung *et al.* 2004; Schumacher *et al.* 2005; Kushnir *et al.* 2006*b*) and

moderate (She *et al.* 1993; Wang *et al.* 1999, Vedula, Yeung & Fox 2001) Reynolds-number range, with perhaps the exception of Yeung, Donzis & Sreenivasan (2005). However, they all tackle the problem of turbulent mixing in its simplest form, i.e. between passive scalars. Donzis, Sreenivasan & Yeung (2005) give a good account of the attributes of such DNS studies to date. For the low-to-moderate Reynolds-number range evidenced in the present DNS, the small-scale evolution for reacting cases can be expected to differ markedly from the evolution in non-reacting cases owing to dilatation and relaminarization of the flow. DNS of constant-density flows can therefore not be used to quantify dissipative structures in reaction zones for such Reynolds numbers. However, DNS studies for the complex case of turbulent mixing with reaction, e.g. in the aforesaid case of turbulent jet flames (Boersma 1999) or in channel flows (Brethouwer & Nieuwstadt 2001), tend invariably to be limited to the low-to-moderate range of Reynolds numbers with simplified chemistry and resolution limited to about $\eta$. Even the relatively good resolution of the turbulent diffusion flame DNS by Mizobuchi *et al.* (2005), using a varying 23–400 million grid-point computational domain, is incapable of reproducing intermittency effects accurately owing to the high Reynolds number it attempts to simulate and is, therefore, unsuitable for our present purpose.

Therefore, we have chosen an extremely well-resolved DNS of a turbulent reacting jet at a moderate jet-exit Reynolds number of 3000 and with relatively detailed four-step chemistry (Pantano 2004). This DNS models the jet flow in the region important for flame stabilization close to the nozzle. The near-nozzle region of jet flames has remained virtually unstudied with respect to the scaling laws for the estimation of the smallest turbulence scales, but a better understanding of the spatial-resolution requirements for scalar dissipation in the stabilization region of the jet flame may be as important as the well-studied self-similar regions further downstream. It is important to note that Kolmogorov's first hypothesis regarding the universal behaviour of the fine dissipation length scales holds in the low-to-moderate Reynolds-number range (She *et al.* 1993; Nelkin 1994; Saddoughi & Veeravalli 1994; Pope 2000; Yeung *et al.* 2004; Kushnir *et al.* 2006*b*, Wang, Karpetis & Barlow 2007*b*). This justifies the rationale of the present study that concerns itself with the spatial scales of dissipation and does not depend on the existence of a well-defined inertial subrange in the turbulence spectrum. See §§ 4.2 and 4.3 for further discussion on this important issue.

### 3.2. *Relevant attributes of the simulation*

The present study makes use of the extensive database of a three-dimensional DNS of a spatially evolving planar turbulent jet by Pantano (2004). The simulation models the non-premixed combustion of methane with air using a four-step reduced mechanism in which the transport equations for eight chemical species and five fluid mechanical fields are solved. The DNS solves the compressible Navier–Stokes equations for moderately low Mach number (i.e. with negligible compressibility effects) on a large cuboidal computational grid of $(N_x = 1024) \times (N_y = 512) \times (N_z = 192)$ grid-points, where the $x$-, $y$- and $z$- Cartesian coordinate axes are aligned with the streamwise, cross-stream and spanwise directions, respectively.

Figure 1 shows the schematic of the computational domain. The attributes of the DNS are given in table 1. Here, $U_j$ is the efflux velocity of the jet, $\Delta u = U_j - U_c$ is the velocity difference (at efflux) between the co-flow and the jet, $c_1$ and $c_2$ are the speeds of sound in the respective streams, $\nu_0$ is the kinematic viscosity of air at STP conditions and $\Phi$ is the fuel–air equivalence ratio. The value of the stoichiometric mixture fraction, $Z_s$, in the present DNS is four to eight times larger than that for pure

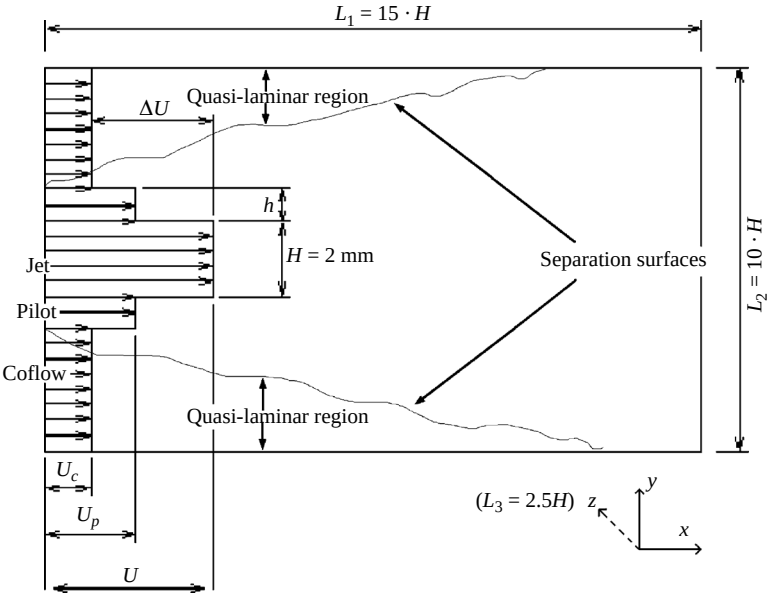


FIGURE 1. Schematic of the computational domain. The spanwise dimension $L_3$, not shown here, is orthogonal to the plane of the figure.

| | | |
|---|---|---|
| *Geometrical attributes* | | |
| Nozzle width | $H$ | $\sim$2 mm |
| Pilot width | $h$ | $0.325\,H$ |
| Computational box dimensions | $(L_1, L_2, L_3)$ | $(15\,H, 10\,H, 2.5\,H)$ |
| *Physical attributes* | | |
| Co-flow and pilot velocities | $U_c,\ U_p$ | $0.029\,U_j,\ 0.29\,U_j$ |
| Convective Mach number | $M_c = \Delta u/(c_1 + c_2)$ | 0.3 |
| Jet-exit Reynolds number | $Re = \Delta u H/\nu_0$ | 3000 |
| Centreline Taylor Reynolds numbers | $Re_\lambda = \sqrt{6.667 Re_\delta}$ | 38 to 58 |
| Prandtl number for air | $Pr = \nu/D_T$ | 0.7 |
| Stoichiometric mixture-fraction | $Z_s = 1/(\Phi + 1)$ | 0.2 |

TABLE 1. Geometrical specifications of the computational domain of the analysed DNS, including the general physical attributes of the simulated flow. The Taylor Reynolds number dependence on the outer-scale Reynolds number, $Re_\delta$, is defined according to Pope (2000).

hydrocarbon–air flames owing to the dilution of the hydrocarbon fuel with nitrogen. The Lewis number, $Le = \alpha/D$, where $\alpha$ is the thermal diffusivity, is unity for the mixture-fraction field. This implies a Schmidt number equal to the Prandtl number, $Sc = Pr = 0.7$. This DNS uses a compact Padé scheme with sixth-order accuracy for the computation of the spatial derivatives (Lele 1992). This scheme provides an improved resolution of the finer length scales without numerical dissipation. Pre-empting one of the results of this study, we note that the grid-discretization employed in the DNS is fine enough to capture the instantaneous $\chi$-distribution. This can be deduced from the distribution of the grid-normalized dissipation length scales that are shown in figure 13.

For the studied flow configuration, the outer-scale Reynolds number, $Re_\delta$, is defined as:

$$Re_\delta = \frac{\delta_{0.5} u'}{\nu}, \tag{3.1}$$

where $\delta_{0.5}$ is the outer-scale of the flow, proportional to the integral-scale of turbulence and computed as the jet half-width, i.e. the distance between the points where the average jet velocity falls to half its centreline value. Here, $u'$ is the representative value of the turbulent velocity fluctuations and $\nu$ is the local kinematic viscosity. This parameter is used throughout the paper to parameterize the dependence of the dissipation length scales on Reynolds number, as is customary in turbulence theory. Depending on the method of computation of the (instantaneous or mean) scalar dissipation length scales (cf. § 2.1), the $u'$ value at any location will be taken as the instantaneous value or as the root-mean-square of the local distribution, respectively. Further details on the flow configuration and its numerical implementation can be found in Pantano (2004).

It remains to say that the character of the simulated jet flame implies that a sizeable number of data points in the quasi-laminar region outside the separation surfaces of the jet will not be relevant for the computation of the dissipation length scales. An estimate of the region that contributes significantly to the data-processing algorithms can be based on the normalized correlation coefficient of scalar fluctuations, $C_Z(x_c, y_c, r)$ (cf. Appendix A). The regions, where $|C_Z(x_c, y_c, r)|$ remains monotonically less than 1% of its centreline value of unity, correspond to quasi-laminar regions. Here, the flow is largely uncorrelated with the turbulence within the jet and therefore does not affect the dissipation of scalar fluctuations. Based on this measure, about 75% of all data points contribute to the computation of the dissipation length scales. It shall be noted, however, that none of the methods introduced in § 2.2 and described in the following sections explicitly discards the quasi-laminar region of the computational domain for post-processing.

## 4. Spectral analysis

### 4.1. *Cross-stream scalar-dissipation spectra*

The spectral theory of the turbulent velocity field has a direct analogy in turbulent scalar fields (Batchelor 1959; Tennekes & Lumley 1974). For sufficiently high Reynolds numbers and Schmidt numbers close to unity, the form of the scalar spectra is similar to that of the velocity spectra.

In the present study, the one-dimensional scalar spectra, $E_Z(k_y)$, at wavenumber $k_y$ is computed as the one-dimensional Fourier transform of the two-point cross-stream correlation, that is equivalent to the power spectrum of scalar fluctuations (Tennekes & Lumley 1974; Pope 2000) at various downstream locations. The details on the computation of the one-dimensional turbulence dissipation spectrum are given in Appendix A. The choice of locations for the spectral analysis is limited by the evolving nature of the simulated turbulent jet, where large portions of the upstream flow domain on either side of the jet are quasi-laminar (Pantano 2004). Therefore, scalar correlations in such regions are of little interest. Owing to these constraints, the region along the centre of the evolving turbulent jet was chosen for the spectral analysis, where the local turbulent Reynolds-number values are high enough for the existence of a 'universal' dissipation range (cf. §§ 4.2 and 4.3).

It is recognized that the one-dimensional cross-stream spectra do not account for the streamwise and spanwise contributions of mixture fraction gradients to the total scalar dissipation. However, determination of the absolute values of scalar dissipation is not of primary concern here since the length scales will be determined by the largest gradients, some of which will be aligned with the cross-stream direction. In planar-jet turbulent flow (with purely streamwise forcing of the jet) the thin shear layers and, therefore, the thin and elongated scalar dissipation structures are predominantly orthogonal to the cross-stream direction in the near-nozzle region. Thus, the cross-stream scalar spectra are able to capture the average scales (or the average thicknesses of these structures) at which scalar fluctuations are dissipated for this flow. In addition, the grid resolution is finest in this direction, enabling the computation of $E_Z(k_y)$ at the highest possible wavenumbers. Note, however, that the dissipation field becomes nearly isotropic far downstream (Buch & Dahm 1998; Su & Clemens 2003) and one-dimensional cross-stream spectra may not capture the smallest scales there.

### 4.2. *Batchelor length-scale computation*

The 'universal' dissipation subrange of the standard non-reactive spectral theory of turbulence is defined as the region in wavenumber space beyond the diffusive roll-off limit. In terms of the non-dimensionalized wavenumber, $k^*$, which is computed by multiplying the wavenumber with the Kolmogorov- or Batchelor-scale, this subrange starts at $k^* \simeq 0.1$ (Pope 2000). A comparison of various experimental results in Saddoughi & Veeravalli (1994) shows that the scaled one-dimensional spectra collapse onto a single curve at $k^* > 0.1$ for Taylor Reynolds numbers between 23 and 3180. In other words, they show a 'universal' dissipation range scaling. Furthermore, it is observed that the scaled one-dimensional dissipation spectrum (Pope 2000) peaks at $k^* \simeq 0.26$. Since the peak value occurs at $k^* > 0.1$, it can be used to define a spectral estimate of the Kolmogorov or Batchelor length scale for the aforesaid range of Taylor Reynolds numbers. In the case of the scalar field, an analogy can be used to define a spectral scalar dissipation scale, according to

$$\eta_{Z_s} = \frac{[k^*]_{peak}}{k_{peak}} \simeq \frac{0.26}{k_{peak}}, \tag{4.1}$$

where $k_y = k_{peak}$ is the wavenumber of the peak in the computed cross-stream dissipation spectra. It can be shown that the area up to the $k^* = 1.0$ cutoff under the aforesaid one-dimensional dissipation spectrum contributes around 98% to the total mean dissipation. The high-resolution experiments of Wang *et al.* (2007*a*, *b*) use a similar technique to arrive at the estimates of the Batchelor scale for axial jet flames at locations $\geqslant 40$ nozzle diameters downstream. The value of the model spectrum of Pope (2000) at $k^* = 1.0$ corresponds to 7.3% of the peak dissipation level. Thus, the inverse of the wavenumber where the dissipation spectrum reaches 7.3% of its peak value is taken as the Batchelor-scale estimate. This wavenumber is denoted $k_{7.3\%}$ and the corresponding Batchelor-scale estimate is given by

$$\eta_{Z_s} \simeq \frac{1}{k_{7.3\%}}. \tag{4.2}$$

Wang *et al.* (2007*a*, *b*) use a somewhat more stringent estimate based on the wavenumber where the spectrum reaches 2% of its peak value.

Figure 2 shows the computed non-dimensional scalar dissipation spectra. On scaling the wavenumber range for the dissipation spectra with $\eta_{Z_s}$ obtained from (4.2), it

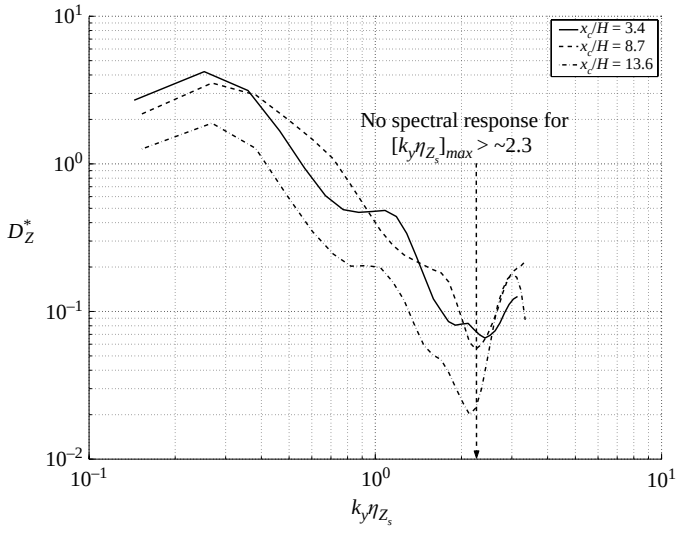


FIGURE 2. Scalar dissipation spectra in logarithmic coordinates at various downstream locations. The horizontal axis denotes the non-dimensional wavenumber $k_y\eta_{Z_s}$ and the vertical axis denotes the normalized scalar dissipation spectra, $D_Z^* = D_Z(k_y)/(\langle D\rangle\langle\chi_y\rangle\langle\epsilon\rangle^{-1/3}\eta_{Z_s}{}^{-1/3})$. The spectra were initially computed for 512 closely spaced values of $k_y$ and averaged into 30 'bins' in the wavenumber space.

is evident that the numerical cutoff limit in the spectra does not set in until well beyond the Batchelor scale (i.e. at $k_y\eta_{Z_s} \simeq 2.3$). As expected, the peaks for the non-dimensionalized spectra occur at $k_y\eta_{Z_s} \simeq 0.26$, with a slight shift to lower wavenumbers for $x_c < 5H$. The vertical line indicates the approximate non-dimensional wavenumber limit (around $k_y\eta_{Z_s} = 2.3$) beyond which no more meaningful spectral response is obtained from the database. For wavenumbers beyond this limit, the turbulence energy spectrum becomes flat and represents a 'noise floor' (Wang *et al.* 2007*a*). This in turn corresponds to an increase, proportional to $k_y{}^2$ (cf. Appendix A), evidenced in the dissipation spectra beyond this limit.

The one-dimensional dissipation spectra computed above can be used to extract information regarding the average downstream evolution of the cross-stream scalar dissipation, which in turn provides estimates for the Batchelor length scales at the respective downstream locations. Analogous to the definition of viscous dissipation in wavenumber space, the average scalar dissipation at any downstream centreline location can be recovered from the integral of the one-dimensional dissipation spectrum at that location (Tennekes & Lumley 1974; Mathieu & Scott 2000; Pope 2000). The spectral estimate (denoted by the subscript $s$) of the average scalar dissipation rate is, therefore, given by

$$\langle\chi_y\rangle_s = 2\int_0^\infty D_Z(k_y)\,\mathrm{d}k_y, \tag{4.3}$$

where $D_Z$ is defined in Appendix A. The above identity is consistent with the factor of 2 used in (1.1). It must be noted that the spectral estimate of the average scalar dissipation rate corresponds only to the dominant cross-stream component of $\langle\chi_y\rangle$ given by the spatial-gradient along the $y$-coordinate only, i.e. $\langle\chi_y\rangle = \langle 2D\,(\partial Z/\partial y)^2\rangle$. As expected, there is good agreement between the jet-centreline averaged scalar

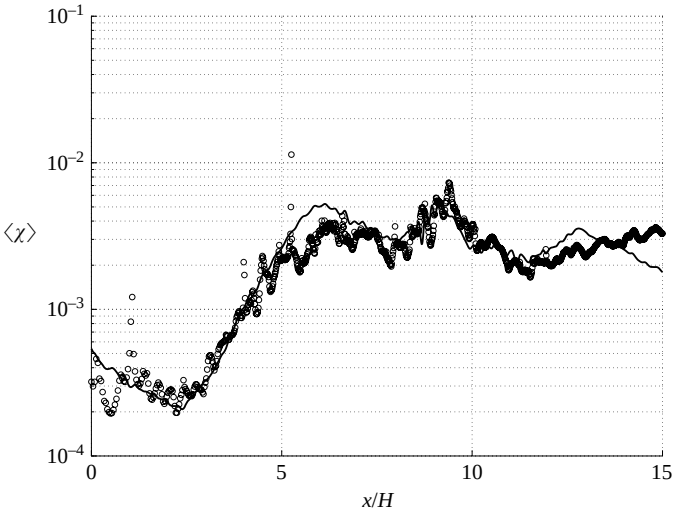


FIGURE 3. Comparison of the downstream evolutions (along the jet centreplane) of the averaged scalar dissipation rates: —, calculated from cross-stream scalar gradients, $\langle\chi_y\rangle$, and ○, recovered from one-dimensional dissipation spectra, $\langle\chi_y\rangle_s = 2\int D_z\,\mathrm{d}k_y$.

dissipation rate from spatial and spectral calculations, as functions of the downstream coordinate (figure 3).

### 4.3. *Reynolds-number scaling*

The non-reacting experimental data in Saddoughi & Veeravalli (1994) show that the departure from the universal behaviour at low Reynolds numbers arises mainly in the energy-containing range (roughly $k^* > 0.003$), while the inertial-subrange (roughly $0.003 < k^* < 0.1$) is diminished. However, as described in §4.2, the whole range of Reynolds numbers exhibits a 'universal' dissipation-range scaling at $k^* > 0.1$ (Nelkin 1994; Pope 2000) and shows excellent agreement with the non-dimensional spectrum.

A numerical simulation of isotropic turbulence by She *et al.* (1993) showed that the scaled spectra fall onto a universal curve at $k^* \geqslant 0.03$ for Taylor Reynolds numbers in the range of $15 \leqslant Re_\lambda \leqslant 200$. In addition, the DNS study of turbulent scalar mixing by Yeung *et al.* (2004) shows that Kolmogorov's first hypothesis regarding the dissipation range of the energy spectrum and, thus, its scaling given by (2.1) holds at Taylor Reynolds numbers between 8 and 38. The same scaling is obtained by Kushnir *et al.* (2006*b*) for dissipation 'filament' thicknesses when Taylor-scale Reynolds numbers equal 10 and 24. Hence, for our present case where $Re_\lambda$ varies from around 20 to 67 throughout the computational domain (and from 38 to 58 along the centreline), it is expected that the spatial scales in the dissipation range still possess the 'universal' behaviour associated with Kolmogorov's first hypothesis, despite the diminished inertial subrange at such low-to-moderate Reynolds numbers.

Conventionally, the finest mixing-length scale is associated with the local turbulent Reynolds number, $Re_\delta$, and Schmidt number via the relationship

$$\frac{\eta_Z}{\delta_{0.5}} = \Lambda_0 Sc^{-3/4} Re_\delta{}^{-3/4}, \tag{4.4}$$

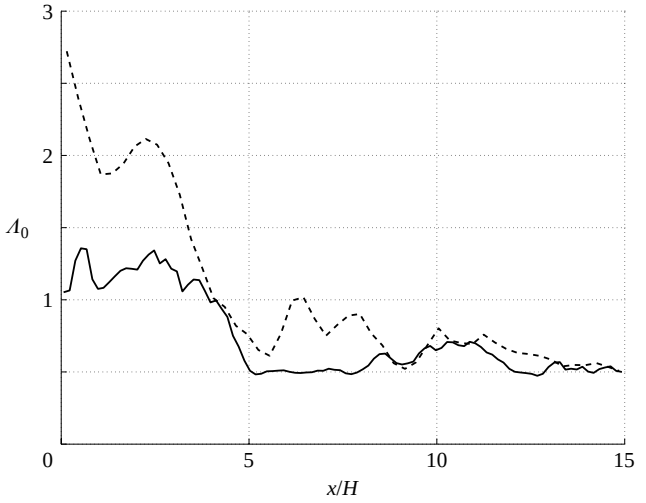


FIGURE 4. Downstream variation of $\Lambda_0$ values is computed by replacing $\eta_Z$ with its spectrally recovered value $\eta_{Z_s}$ from - - -, (4.1) and —, (4.2).

where $\Lambda_0$ is the proportionality constant or the scaling coefficient. This relationship is based on dimensional arguments and it must be noted that the $Re_\delta$-scaling in the above definition follows from Kolmogorov's first hypothesis, which holds (as remarked above) at the Reynolds numbers that can be found in the present DNS. The Batchelor-scale definition in Pitts *et al.* (1999) assumes the left-hand side in the above equation, i.e. $\eta_Z/\delta_{0.5}$, to be of the same order-of-magnitude as $Sc^{-3/4}Re_\delta{}^{-3/4}$ implying that $\Lambda_0 \simeq 1$. It should also be noted here that other experimental studies (Buch & Dahm 1998; Su & Clemens 2003) give values of $\Lambda_0$ in the range of 5 to 11 for the far-downstream self-similar regions of the jet.

To confirm the $Re_\delta$-scaling of (4.4) for the present study, the $\eta_Z$ term is substituted by its spectral estimate $\eta_{Z_s}$ from (4.1) and (4.2) along the jet centreline. The resulting values of the scaling coefficient, $\Lambda_0$, are then plotted as functions of the downstream positions in figure 4. The values computed using (4.1) oscillate slightly around a constant mean value of $\Lambda_0 \simeq 0.7$, except in the near inflow region ($x_c < 5H$) of the developing jet flow, where cross-stream inhomogeneities are severe and the statistics of the velocity field are poorly reflected in those of $Z$. The $\Lambda_0$ values from (4.2) show a similar downstream evolution, however, with appreciably fewer fluctuations and remain around 0.5 for locations $x_c \geqslant 5H$.

In the region upstream of $x_c = 5H$, the jet core has not broken up yet and there is a low amount of scalar mixing along the centreline. Consistently, the small scalar dissipation rate (i.e. the dissipation spectrum being confined to a relatively small range of wavenumbers) results in an over-estimation of the Batchelor scale from (4.1) and (4.2). This seems to be in agreement with the results from the DNS by She *et al.* (1993), where the computed $k_{peak}$ wavenumber was found to be slightly smaller (at lower Reynolds numbers) than the proportionality to $1/\eta_Z$ would imply. In other words, the Kolmogorov scale based on $0.26/k_{peak}$ is somewhat over-estimated when Taylor Reynolds numbers are low. However, the roughly constant values of $\Lambda_0$ seen for most of the downstream section ($\geqslant 5H$) in figure 4, corroborate the finding that the spectrally computed estimates using (4.2) are representative of the Batchelor length scales in the flow.

## 5. Direct computation of scalar dissipation structures

We use a measurement method that is similar in spirit to the experimental technique described in Su (1998) and Su & Clemens (2003). Here, we investigate directly the thin sheet-like three-dimensional regions aligned with the regions of high shear within the computational domain, where most of the scalar dissipation process remains concentrated (Buch & Dahm 1998; Tsurikov & Clemens 2002). Notable numerical studies of the small-scale topological structure of the turbulent scalar/dissipation field have been done by Wang & Peters (2006) and Kushnir *et al.* (2006*b*). In the former study, the approach has been to identify the regions, termed as 'dissipation elements', of monotonic increase (or decrease) of the fluctuating scalar concentration. Analysis of these 'dissipation elements' also confirms a high probability of alignment between scalar gradients and the most compressive rate of strain, as found in the shear layers of the turbulent jet flow. Kushnir *et al.* (2006*b*) analyses the topology of the two-dimensional scalar-dissipation-rate field using a sophisticated numerical algorithm (Kushnir *et al.* 2006*a*). For all points on the two-dimensional field belonging to the regions delineated by a threshold value of the dissipation level-set, the algorithm computes a so-called 'proximity graph', which is updated on successive coarse-graining and can be used to quantify statistical properties such as the density and convexity of the points at each level of resolution. Finally, a principal component analysis is carried out on these dissipation 'filaments' or 'sub-filaments' identified on the basis of the aforementioned statistical properties. The filament thickness is thus characterized by the eigenvalue of the eigenvector orthogonal to the direction of orientation of the filament.

### 5.1. *Algorithm*

An algorithm previously used by Buch & Dahm (1998) and Su & Clemens (2003) for the computation of the two-dimensional (planar) dissipation-layer thicknesses with a correction for their three-dimensional orientation has been employed in the present study. The dissipation layers are identified as the contours or level-sets at fixed values of $\chi$ within the instantaneous $\chi(x, y)$ field. The fixed values are chosen as a fraction, $\beta_m$, of the local maxima in their neighbourhood $(x, y)$ locations. The local thickness of a dissipation layer, $\lambda_{2d}$, at a given value of $\beta_m$ quantifies the instantaneous two-dimensional dissipation length scale. This two-dimensional dissipation length-scale estimate is then corrected by using the three-dimensional orientation of the scalar gradient vector in terms of the out-of-plane angle, $\phi$, to give the three-dimensional length-scale estimate, $\lambda_{3d}$. The algorithm and all the parameters involved are described in more detail in Appendix B and figure 15 illustrates the procedure.

It is worth noting that the present algorithm introduces some simplifications in the computations of the dissipation-layer thicknesses and it differs from the algorithm used by Buch & Dahm (1998) and Su & Clemens (2003) in two aspects. First, the two-dimensional neighbourhood regions that define the dissipative structures may include more than one local maximum of $\chi$ for very low values of $\beta_m$. As a result, these regions would appear longer (more elongated) than the dissipation regions identified by Buch & Dahm (1998). Secondly, we do not account for the variation in the 'local layer-normal dissipation maximum' (see Buch & Dahm 1998 for its definition) along the dissipation layer and this leads to thinner structures than reported in Buch & Dahm (1998). However, owing to our choice of relatively high values for $\beta_m$ (cf. Appendix B), the neighbourhood regions tend to isolate the local maxima and the computed dissipation-layer thicknesses will be similar for the two algorithms. In other words, the differences between the dissipation-layer thicknesses reported from both algorithms will decrease with increasing $\beta_m$.

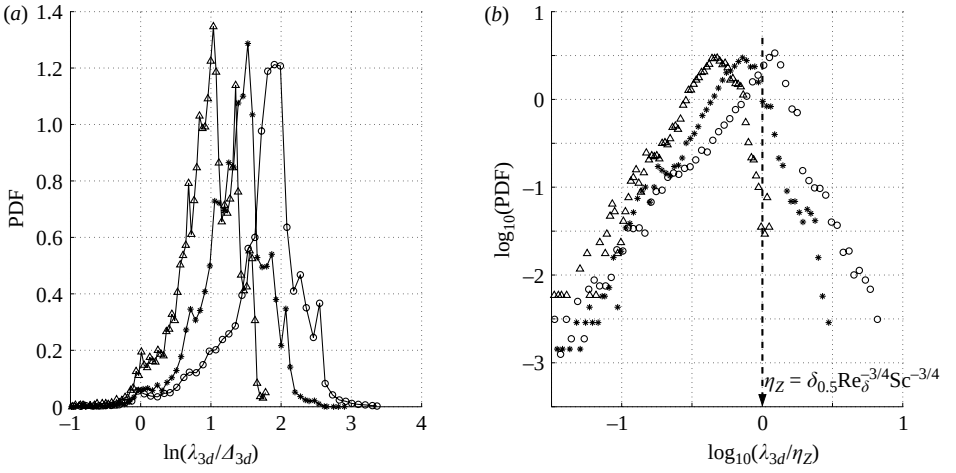


FIGURE 5. (*a*) PDFs of the logarithm of the corrected (three-dimensional) scalar dissipation-layer thicknesses are normalized with the effective grid-discretization $\Delta_{3d}$ for $\beta_m = 0.5$, 0.75 and 0.9. The negative values for $\ln(\lambda_{3d}/\Delta_{3d})$ are numerical artefacts due to the thicknesses computed at the very few locations where $\phi \to 90°$. (*b*) PDFs of $\lambda_{3d}$ are normalized by the dissipation length scale $\eta_Z$ from (4.4) with a unity scaling coefficient. ○, $\beta_m = 0.5$; ●, 0.75; △, 0.9.

Figure 5(*a*) shows the distribution of the corrected scalar dissipation-layer thicknesses, $\lambda_{3d}$, normalized by the local grid-discretization, $\Delta_{3d} = \left(\Delta_x \Delta_y \Delta_z\right)^{1/3}$, in the computational domain. The effective three-dimensional grid-spacing is denoted by $\Delta_{3d}$, where $\Delta_x$, $\Delta_y$ and $\Delta_z$ are the variable grid-discretizations in the respective coordinate directions. The detection of values smaller than the minimum grid-spacing limit can be primarily associated with locations where the out-of-plane angle $\phi$ tends to 90°. This phenomenon is also amplified by the interpolation between grid points near the corners of the dissipation layers when computing the iso-contours. However, owing to the small number of such occurrences (cf. figure 16 in Appendix B), their effect on the analysis is negligible.

In figure 5(*b*), the PDFs of the dissipation-layer thicknesses normalized by the magnitude of the local dissipation scale, $\eta_Z$, show negative skews at all values of $\beta_m$. In other words, dissipation length scales smaller than the most frequently occurring scale (given by the peak of each PDF) are more likely to occur than those larger than the most frequently occurring scale. This is in agreement with the results in Kushnir *et al.* (2006*b*), where a similar negative skew is observed in the normalized dissipation 'filament' thicknesses. In addition, figure 5(*b*) shows that the formation of dissipative structures with thicknesses of the order of $\eta_Z$ is conditional on the chosen value of $\beta_m$. However, this dependence on $\beta_m$ or any equivalent measure of spatial resolution is not apparent in the analysis by Kushnir *et al.* (2006*b*). A majority of their computed dissipation 'filaments' are reported to be thicker than $\eta_Z$, an observation limited to lower $\beta_m$ values in the present analysis.

Schumacher *et al.* (2005) used scalar increments over the viscous convective range between the Kolmogorov and Batchelor scales (for $Sc > 1$) which yielded a dissipation-scale estimate slightly greater than $\eta_Z$. However, unlike Kushnir *et al.* (2006*b*), the actual distribution of dissipation length scales is not captured in this analysis and this approach is therefore not used here.

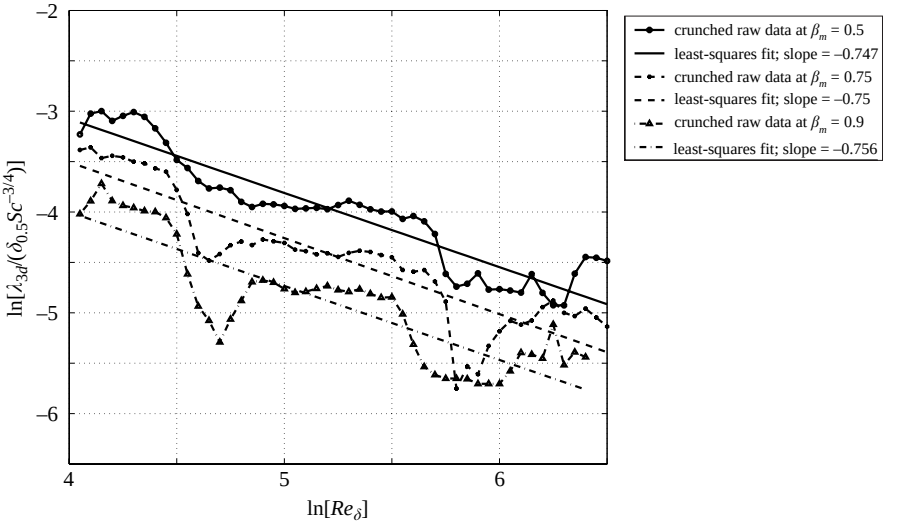


FIGURE 6. Observed $Re_\delta{}^{-0.75}$ scaling dependence for the corrected dissipation-layer thicknesses, $\lambda_{3d}$ in log–log coordinates. Data corresponding to a single computational time step is shown at $\beta_m = 0.5$, 0.75 and 0.9.

### 5.2. *$Re_\delta$-scaling of dissipation-layer thicknesses*

In this section, we use a local Reynolds-number definition where $u'$ represents the local velocity fluctuation. This is necessary in order to account for the fluctuating nature of $\lambda_{3d}$ and the necessity to relate instantaneous scales with Reynolds numbers based on instantaneous or local quantities. This is opposed to the analysis in § 4.3 where a quantity computed from two-point correlations such as the dissipation spectrum requires Reynolds numbers based on averaged quantities such as the r.m.s. Figure 6 shows the scalar dissipation thickness as a function of Reynolds number. The whole range of $Re_\delta$ values is grouped into 60 bins and is plotted against the bin-average of $\lambda_{3d}/\left(\delta_{0.5}Sc^{-1/2}\right)$ in log–log coordinates. The least-squares fits for several values of $\beta_m$ show a negative slope that approximates the value $-0.75$. This is consistent with a Kolmogorov-type or $Re_\delta{}^{-3/4}$ scaling that is independent of $\beta_m$ and the findings are in agreement with the experimental and numerical results of Buch & Dahm (1998), Su & Clemens (2003) and Kushnir *et al.* (2006*b*).

It is important to note that the number of data samples for the dissipation-layer thicknesses, i.e. the number of spatial locations within the computational domain where the thicknesses have been computed, decreases with increasing $\beta_m$ as resolution constraints increase. For example, the sample size for $\beta_m = 0.5$, 0.75 and 0.9 is around 40 000, 30 000 and 9 000 points, respectively. Furthermore, the distribution of samples becomes increasingly discontinuous over the streamwise direction and hence over the $Re_\delta$-space at higher $\beta_m$ values, owing to correspondingly thinner layers. Therefore, the plots show larger variation around the least-squares fit at larger $\beta_m$ values.

### 5.3. *Variation of scaling coefficient with $\beta_m$*

Assuming the existence of a $Re_\delta{}^{-3/4}$ scaling of the dissipation-layer thicknesses as evidenced in figure 6, the current formulation for $\lambda_{3d}$ can be assumed to scale (similar to (4.4)) as

$$\lambda_{3d} = \Lambda_{3d}\delta_{0.5}Sc^{-3/4}Re_\delta{}^{-3/4}, \tag{5.1}$$

where $\Lambda_{3d}$ is the scaling coefficient for the dissipation length scales, when expressed in terms of corrected three-dimensional scalar dissipation-layer thicknesses. Values of the scaling coefficient, $\Lambda_{3d} \simeq 1.2$ *to* 0.55 determined by (the exponential of) the $y$-intercept of the least-square fits shown in figure 6, are observed to decrease over the investigated local $\chi$-resolution range given by $\beta_m = 0.5$ to 0.9. The scatter around the mean (least-squares) estimate for $\Lambda_{3d}$ is nearly Gaussian-distributed over the whole Reynolds-number range. The standard deviation in the scaling coefficient values is around 30% of the mean for each $\beta_m$ value. Thus, the interval $[0.4\Lambda_{3d}, 1.6\Lambda_{3d}]$ represents the 95.4% confidence interval associated with our $\Lambda_{3d}$ estimates.

Evidently, the values for the scaling coefficient $\Lambda_{3d}$ are smaller than those predicted in Buch & Dahm (1998) and Su & Clemens (2003), though it is of the same order as the $\Lambda_0$ value computed in § 4.3. This may be explained by the following: in Buch & Dahm (1996, 1998) and Su & Clemens (2003) the dissipation-layer thickness is defined as the distance across the layer between points where the dissipation rate is 20% of the local peak-value. This would be equivalent to a $\beta_m$ value of $\beta_m = 20\%$ in the present study. However, we have chosen to compute the dissipation layers at much higher $\beta_m$ values to isolate the most strongly dissipative regions. These regions determine the finest scales in the scalar field, which is a principal goal of this study. Relaxation of $\beta_m$ to values of 20% would result in a thickening of the dissipation layers and would lead to a higher estimate for $\Lambda_{3d}$. Extrapolation of our results to $\beta_m$ values of $0.1 - 0.2$ would yield $\Lambda_{3d}$ of around $5.0 - 4.0$, which is much closer to the experimental estimates in Buch & Dahm (1998) and Su & Clemens (2003). Further contributing factors to the differences are the simplifications in the algorithm described in § 5.1 and the fact that the experimental studies were for the self-similar regions in non-reacting turbulent jet flows. We stress that an exact determination of $\Lambda_{3d}$ is not of primary interest here (and is, in fact, not possible owing to its dependence on $\beta_m$). We seek to establish the validity of scaling relationships for the dissipative structures in turbulent reacting flows with low-to-moderate Reynolds numbers. These scaling relationships appear to be similar to scaling laws established for non-reacting flows.

## 6. Spatial-filtering analysis

Adequate spatial resolution to capture scalar dissipation means that the scalar gradient should remain sufficiently unchanged over the minimum length scale of discretization or experimental probe-width employed for measurement. However, owing to small-scale intermittency, the fluctuations in scalar gradients (and hence in $\chi$) can be many orders of magnitude higher than the mean and have a much higher probability of occurrence (i.e. they show a lognormal-like PDF) than those in the scalar (Sreenivasan 2004). Sreenivasan (2004) proposes that the best way to deal with an intermittent variable such as $\chi$ is to smooth it locally over a non-overlapping spatial interval (in other words, filter-width, $w_f$). The properties of the smoothed variable can then be studied as a function of $w_f$ as it is extrapolated to the smallest scale of interest. In the present study, we use the analogy of the above approach with the experimental spatial-filtering technique of Barlow & Karpetis (2005*b*, *b*). This is achieved by analysing the decay of the frequently occurring instantaneous spikes in $\chi$ resolved by the DNS as the size, $w_f$, of the applied numerical filter is increased beyond the computational grid-resolution. The type of decay with $w_f$ is used to reconstruct the hypothetical 'fully resolved' $\chi$ peak values corresponding to zero filter width. The ratio of the DNS-resolved instantaneous spikes in $\chi$ to the 'fully resolved' reference limit is investigated.

### 6.1. *Spatial-filtering method*

Previous experimental studies of axisymmetric turbulent jet flames by Barlow & Karpetis (2005*b*) show that the peak value of the logarithm of the mean cross-stream component of $\chi$ decreases linearly with increasing filter width. As explained above, this linear decay is then exploited to calculate the 'fully resolved' limiting value at zero filter width. However, it should be pointed out that in the context of the numerical implementation of this technique to the present DNS, this 'fully resolved' scalar dissipation is a hypothetical maximum that will probably not exist at any point in the simulated flow. This theoretical value strictly serves as a good reference against which the resolution of the spatially filtered $\chi$ peak values is quantified. Thus, a suitable fraction of this reference is subsequently chosen as the effective length scale required for adequate resolution. However, based on the discussion in § 2.1, the instantaneous length scales central to the idea of adequacy of $\chi$-resolution cannot be captured by linear scaling of (the logarithm of) the mean dissipation, but of the instantaneous $\chi$-field that exhibits small-scale intermittency. Therefore, the spatial-filtering method explores the instantaneous cross-stream profiles of scalar dissipation instead.

In the present DNS database, we consider the planar top-hat filtered mixture fraction $Z_f(x, y, z)$ given by

$$Z_f(x, y, z) = \frac{1}{\Delta_{x,f}\Delta_{y,f}} \int_{x-\Delta_{x,f}/2}^{x+\Delta_{x,f}/2} \int_{y-\Delta_{y,f}/2}^{y+\Delta_{y,f}/2} Z(x', y', z)\, \mathrm{d}x'\, \mathrm{d}y', \tag{6.1}$$

where $\Delta_{x,f}$ and $\Delta_{y,f}$ denote the filter width at any $(x, y)$ position, with $w_f = \sqrt{\Delta_{x,f}\Delta_{y,f}}$. For the filtering operation, we drop the $z$-dependence and consider, for simplicity, the scalar dissipation fields at every $(x, y)$-plane as mutually independent realizations. The filtered instantaneous scalar dissipation rate is calculated from the spatially filtered mixture-fraction field at each corresponding grid-point by central differencing of (1.1),

$$\chi_f(x, y, z) = 2D \left( \left[ \frac{\delta_x Z_f}{\Delta_{x,f}} \right]^2 + \left[ \frac{\delta_y Z_f}{\Delta_{y,f}} \right]^2 + \left[ \frac{\delta_z Z_f}{\Delta_z} \right]^2 \right), \tag{6.2}$$

where $\delta_x$, $\delta_y$ and $\delta_z$ are the central-difference operators for the respective coordinate directions. The smallest resolvable filter-width is given by $\Delta = \sqrt{\Delta_x \Delta_y}$, where $(\Delta_x, \Delta_y, \Delta_z)$ is the basic grid-discretization used in the DNS, which varies from location to location owing to the clustering of the grid nodes in regions close to the shear layer. Successive iterations of spatial filtering with successively larger filter-width values will smear out peak values of instantaneous $Z$ (and hence $\chi$).

### 6.2. *Results and discussion*

#### 6.2.1. *Effect of the filter width*

Figure 7 shows that spatial filtering has a strong reducing effect on the instantaneous peaks of scalar dissipation, with the peak value decreasing drastically for increasing filter width. However, the corresponding effect on instantaneous mixture-fraction profiles is practically negligible. If we now assume an exponential decay of the maximum scalar dissipation as suggested by Barlow & Karpetis (2005*b*), it is possible to study the 'fully-resolved' scalar dissipation maxima as the filter width is extrapolated to a sufficiently small value. In other words, we assume a linear variation of the type:

$$\ln(\chi_{f,\,peak}) = \ln(\chi_{0,\,peak}) + s w_f, \tag{6.3}$$

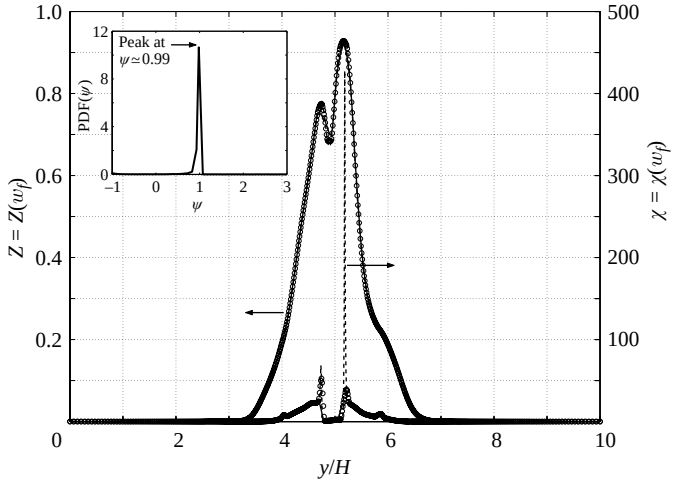


FIGURE 7. Variation of the instantaneous cross-stream profile of scalar-dissipation rate, $\chi$, and mixture-fraction, $Z$, with increasing filter width, $w_f$, at an arbitrarily chosen spatial location ($x/H = 2.8$, $z/H = 0.0$). The peak value of the cross-stream $\chi$ profile appears to drop exponentially with a linear increase in $w_f$. ---, $\omega_f = \sim 0.011$H; ○, $\sim 0.059$H; —, $\sim 0.118$H. The inset shows the PDF of the correlation coefficient, $\psi$, for the least-squares fit between the actual dependence of $\chi$ peak values on $w_f$ and the exponential-decay model in (6.3). $\psi$ is computed for the $\chi$ peak values at $1024/8 \times 192/3 \times 30$ cross-stream profiles throughout the present DNS database. The peak is observed for $\psi \simeq 0.99$. Negative signs have been appended to $\psi$ values to indicate negative linear decay, i.e. for plots with $s > 0$.

where $\chi_{f,\,peak} = max\,(\chi(y))$ is the maximum scalar dissipation value along the cross-stream direction for constant $x$ and $z$ (see figure 7 for illustration), $\ln(\chi_{0,\,peak})$ is the 'fully-resolved' $\chi$ value computed by extrapolating to zero filter width and $s(<0)$ is the slope of decay of the logarithm of the scalar-dissipation peak value. The parameter $s$ quantifies the effect of spatial filtering on the $\chi$ peak value.

For every downstream location, $N_z \times N_T$ realizations can be used to establish the linear relationship described in (6.3), where, $N_T = 30$ is the number of different time instants being considered. Following the method described by Barlow & Karpetis (2005*b*), values of $\ln(\chi_{f,\,peak})$ and the corresponding filter width are accepted only in cases where the linear correlation coefficient of their least-squares fit, $\psi$, is 0.99 or better during the spatial-filtering operation. As is customary, $\psi = 0$ indicates completely uncorrelated variables and $\psi = 1$ implies perfect linear correlation. To reduce the number of cross-stream profiles to be processed from an extremely large value of $N_x \times N_z \times N_T \sim 5.9$ million, one $\chi$-peak per cross-stream profile is assumed for each eighth grid-point along the streamwise direction and each third grid-point along the spanwise direction. Additionally, the condition on $\psi$ limits the large number of available spatio-temporal locations to around 75 500 cases that show near-perfect linearity described by (6.3). The stringent demand on the choice of peak values $\chi_{f,\,peak}$, i.e. $\psi \to 1$ ensures exponential decay with increasing filter width and the important intermittent statistics are thus captured. In addition, the PDF of the $\psi$-values for all the processed cross-stream profiles in figure 7 (inset) shows a high preponderance of values around $\psi \simeq 0.99$. This justifies the validity of the exponential-decay model described by (6.3) in the present DNS.

The following qualitative observations come to light regarding the effects of spatial filtering of the instantaneous $\chi$ profiles. First, the scalar-dissipation values at the 'fully

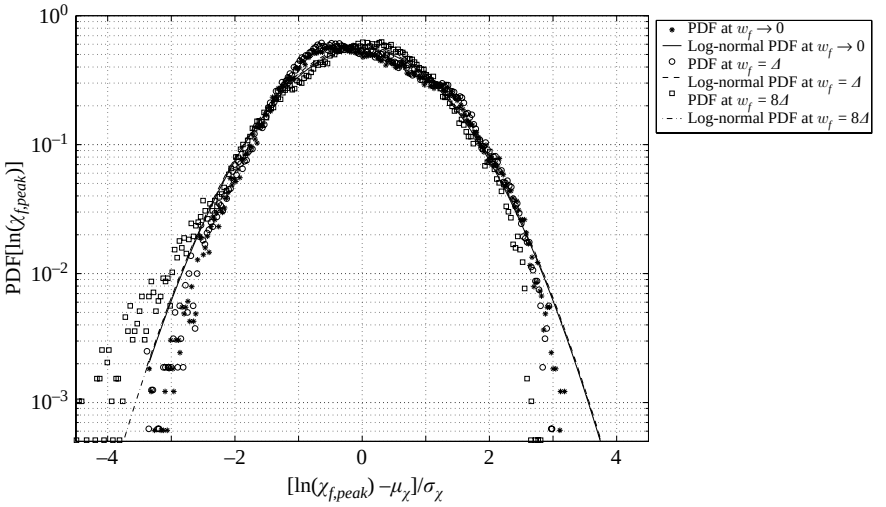


FIGURE 8. Dependence of the PDF of (the logarithms of) the filtered $\chi$ peak values, PDF($\ln \chi_{f,peak}$), on the level of filter width given by the magnitude of $w_f/\Delta$. The symbols show the actual data at various filter widths, whereas the curves show the corresponding log-normal PDFs for the same mean, $\mu_\chi$, and variance, $\sigma_\chi$.

resolved' limit are observed to be finite. Thus, the extrapolation of the peak scalar dissipation values to the 'fully resolved' limit seems valid, as shown by Barlow & Karpetis (2005*b*). Secondly, the PDF of the scalar-dissipation peak value is captured well at the minimum filter width $w_f = \Delta$. Figure 8 compares different PDFs that are obtained by varying the filter width, $w_f$, in (6.1) and (6.2). The figure shows that the PDF of the scalar dissipation values at the 'fully resolved' limit (i.e. $w_f \to 0$) does not show any appreciable change from the PDF captured at the grid spacing (i.e. $w_f = \Delta$), indicating that the DNS grid captures the range of dissipation values quite well. For the larger filter width $w_f = 8\Delta$, the probability distribution shows a negative skewness as the probability of $\chi$-values being smaller than the average increases. Thirdly, on average, the effect of spatial filtering on $\chi$ increases with downstream distance. It peaks at about the centre of the computational domain (around $x/H \simeq 7.5$) beyond which it slightly decreases (figure 9). This seems to be directly linked with the trend shown by the outer-scale turbulent Reynolds number, $Re_\delta$, which also peaks in the centre of the computational domain and decreases slightly further downstream (Pantano 2004). Finally, the magnitude of the spatial-filtering effect, $s$, is sensitive to the corresponding magnitudes of the dissipation peak values resolved by the grid. This is demonstrated in figure 10. The downstream position with the largest average $\chi_{\Delta,peak}$ corresponds to the downstream position with the largest gradient $|s|$, and the downstream position with the smallest average $\chi_{\Delta,peak}$ corresponds to the downstream position with the smallest gradient $|s|$. This correlation holds throughout the flow. This implies that the decay of $\chi$-peaks through filtering is correlated with the magnitudes of these peaks.

The local effects of spatial filtering can be quantified by the parameter $s$ or, equivalently, by the filter widths required for resolving a fixed fraction (defined as $\beta_f$ in (6.5) below) of $\ln(\chi_{0,peak})$. The observations made above imply that these effects are linked to the magnitudes of $\chi$ peak values, which in turn are dependent on the turbulent Reynolds number $Re_\delta$ (Sreenivasan 2004) owing to the intermittent nature of the $\chi$ field. These links are examined in detail next.

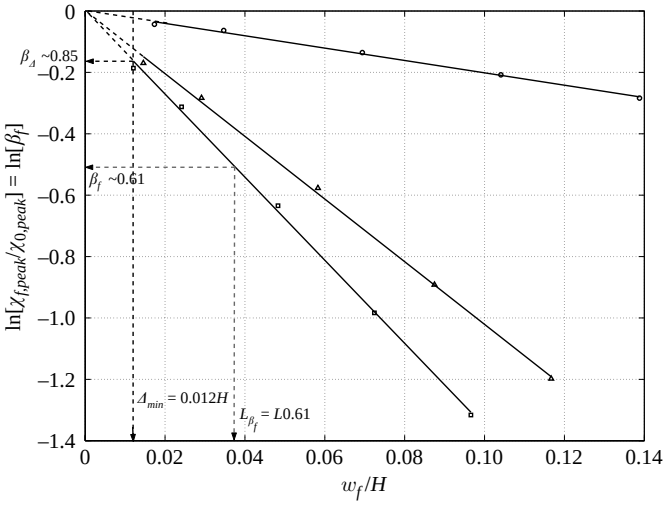


FIGURE 9. Averaged plots of the filtered $\chi$ peak values normalized by the 'fully-resolved' limit with increasing filter width in semi-log coordinates. The reported results indicate the mean variation, computed by averaging over the PDF (of all instantaneous spatio-temporal cases) corresponding to each of the three downstream stations. The horizontal lines indicate 85% and 61% recovery of the 'fully-resolved' $\chi$ value at $w_f = \Delta$ and $w_f = L_{0.61}$, respectively. Here, $\Delta = \sqrt{\Delta_x \Delta_y}$ indicates the non-uniform grid-discretization employed in the DNS. The dotted portions of the linear plots represent the extrapolation at $w_f < \Delta$ and filter widths corresponding to this region do not represent physically resolved dissipation length scales. ○, $x/H = 2.8$; □, 7.5; ▲, 12.1.

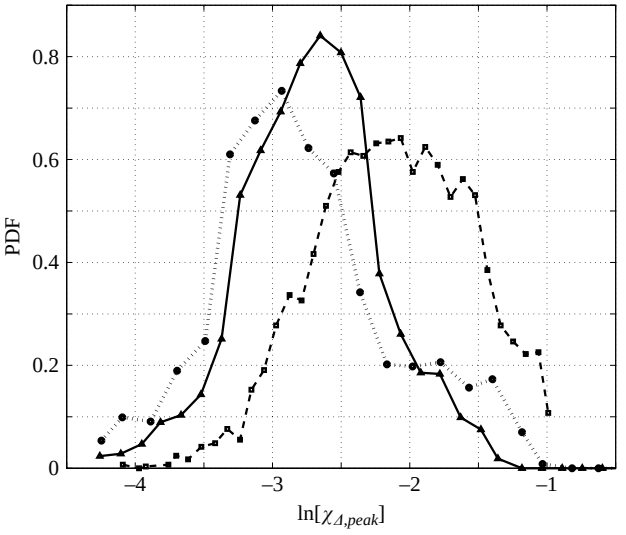


FIGURE 10. Dependence of the PDF of (the logarithms of) the $\chi$ peak values that are resolved by the grid, i.e. PDF($\ln\chi_{\Delta,peak}$) on downstream distance. ●, $x/H = 2.8$; ■, 7.5; ◆, 12.1.

### 6.2.2. *Choice of* $\beta_f$

Following Barlow & Karpetis (2005*b*), we can define a length scale to quantify the effects of spatial filtering on $\chi$. This length scale is the filter width required to recover

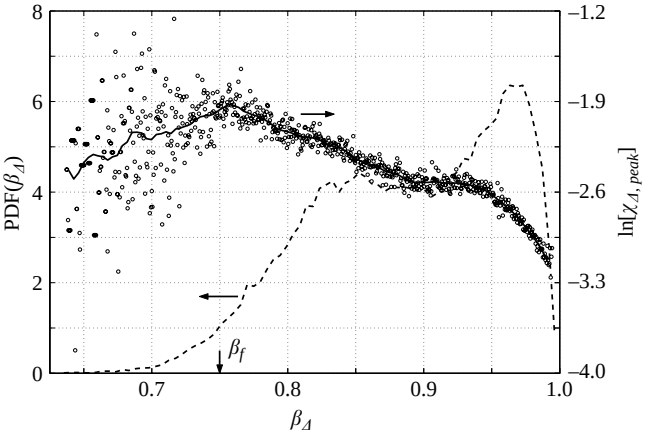


FIGURE 11. Variation of the fraction, $\beta_\Delta$ of the 'fully-resolved' value $\chi_{0,peak}$ recovered by the local grid-discretization (for $\psi > 0.99$) against the (logarithm of) magnitude of the peak value resolved, $\chi_{\Delta,peak}$; ○, scatter-plot data; —, smoothed variation.

a sufficiently large fraction $\beta_f$ of the (hypothetical) 'fully resolved' scalar-dissipation value, where $\beta_f = \chi_{f,peak}/\chi_{0,peak}$. The definition of the length scale $L_{\beta_f}$ then follows from (6.3) as

$$L_{\beta_f} \equiv \frac{\ln(\beta_f)}{s}. \tag{6.4}$$

An appropriate value of $\beta_f$ must be selected in (6.4) in order for $L_{\beta_f}$ to be well defined. The statistics of the fractional value of $\chi_{0,peak}$ that is actually resolved by the computational grid, i.e. the fraction $\beta_\Delta = \chi_{\Delta,peak}/\chi_{0,peak}$ for $w_f = \Delta$, can be used as guidance. Using (6.3), $\beta_\Delta$ can be written as

$$\beta_\Delta = \exp(s\Delta). \tag{6.5}$$

Figure 11 shows the statistics of $\beta_\Delta$ for the whole DNS database. It is evident that the increasingly spiky behaviour of $\chi$ owing to intermittency that is approximated here by the magnitude of the actually resolved peak-$\chi$ values or $\ln(\chi_{\Delta,peak})$, correlates with the decreasing ability of the grid to locally resolve $\chi_{0,peak}$ (i.e. decreasing $\beta_\Delta$). It follows from (6.5) that for a fixed grid-discretization, $\Delta$, the parameter $\beta_\Delta$ depends directly on the rate of spatial-filtering decay, $s$. Therefore, the correlation of $\beta_\Delta$ with $\chi_{\Delta,peak}$ in figure 11 corroborates the preliminary observation made in § 6.2.1 that larger $\chi$ peak values tend to decay faster with filtering. In addition, figure 11 shows that most of the strongest spiky behaviour (or largest $\ln\chi_{\Delta,peak}$ values) occurs in the vicinity of $\beta_\Delta \simeq 0.75$. Thus, in the context of the present DNS, we need not relax the definition of $\beta_f$ below 0.75 for it to be deemed sufficient to capture the strongest dissipative events.

The few spatio-temporal locations (around 2% of the total), characterized by $\beta_\Delta < (\beta_f = 0.75)$ in the PDF on figure 11, correspond to the extrapolated region shown in figure 9. Therefore, the dissipation length-scale values, computed in terms of the filter width at these locations, remain less than the local grid-size. However, these numerical artefacts are insignificant in number and have negligible effect on the analysis.

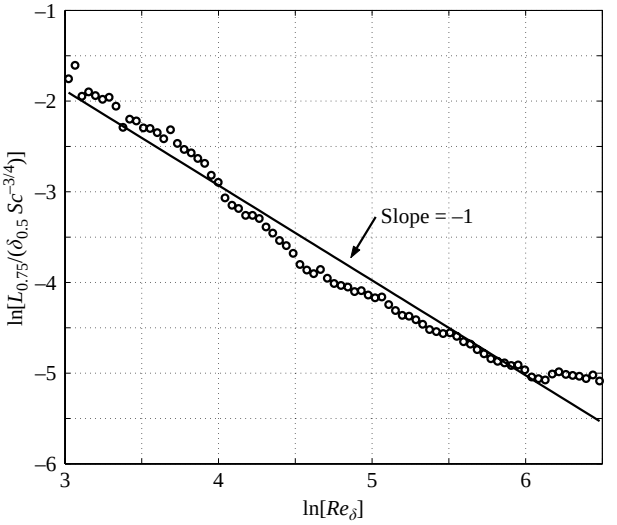


FIGURE 12. Linear scaling of $L_{0.75}/\left(\delta_{0.5}Sc^{-3/4}\right)$ with $Re_\delta$ in double-logarithmic coordinates. A slope of $-1$ is obtained after a least-squares fit. ○, binned and averaged data; —, least-squares fit; $y$-intercept $\sim$1.1.

### 6.2.3. *$Re_\delta$ scaling*

Based on the spatial-filtering analysis of the scalar dissipation field, we can see that the defined length scale $L_{\beta_f}$ is a representative measure of a wide variety of local dissipative events at $\beta_f = 0.75$. Examination of the scaling of the local instantaneous dissipation length scale, $L_{0.75}$, with Reynolds number requires a parameterization at each spatio-temporal location. For the present analysis, the instantaneous $Re_\delta$ is again used, based on the fluctuating velocity component, $u'$, instead of its root-mean-square value. This is consistent with the remarks made earlier in § 5.2.

As commented in § 2.1, many previous studies on the resolution requirements for $\chi$ (e.g. Buch & Dahm 1996, 1998; Pitts *et al.* 1999; Su & Clemens 2003, infer that the minimum length scale deemed adequate to characterize scalar dissipation is proportional to (if not of the same order as) the Batchelor scale. However, it follows from the discussion in the preceding sections that the length scales, $L_{0.75}$, representative of the instantaneous scalar dissipation peaks captured by the spatial-filtering technique, are equivalent to the local, minimum dissipation length scales of Sreenivasan (2004) or $\eta_{Z_{min}}$, that must be resolved for capturing the intermittency of scalar dissipation. The Reynolds-number scaling for these minimum length scales can be established by plotting $\ln(L_{0.75}/(\delta_{0.5}Sc^{-3/4}))$ as a function of $\ln(Re_\delta)$. Because of the large number of data points involved, we divide the $\ln(Re_\delta)$ range into 100 bins and plot the averaged value of $L_{0.75}/(\delta_{0.5}Sc^{-3/4})$ against that of $\ln(Re_\delta)$ for each bin. The result is shown in figure 12 and the data reveal a slope of $-1$ in the double logarithmic plot. We therefore suggest an ${Re_\delta}^{-1}$ scaling for the length scale $L_{0.75}$:

$$L_{0.75} = \Lambda\delta_{0.5}Sc^{-3/4}{Re_\delta}^{-1}. \tag{6.6}$$

This is consistent with scaling estimates for $\eta_{Z_{min}}$ by Sreenivasan & Meneveau (1988) and Sreenivasan (2004) which are based on the theory of multifractals. A similar ${Re_\delta}^{-1}$ scaling estimate for the intermittent dissipation length scales has also been derived by Yakhot (2003) using the theory of turbulence structure functions. The

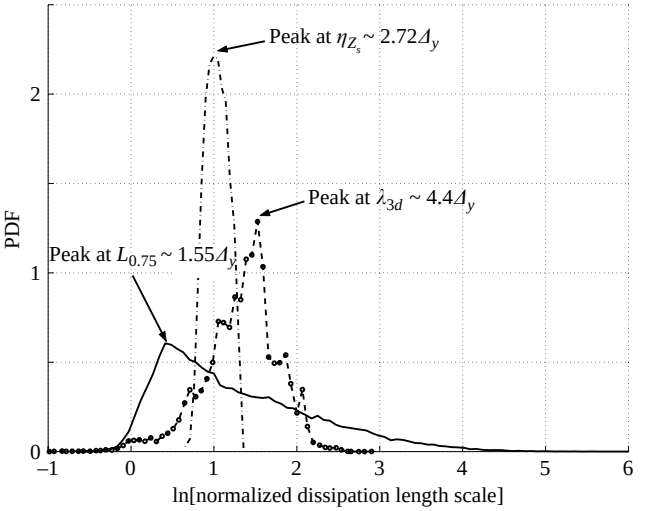


FIGURE 13. PDF of the normalized instantaneous and mean dissipation length scales and dissipation-layer thicknesses, namely, $\eta_{Z_s}$, $L_{0.75}$ and $\lambda_{3d}$ (computed at $\beta_m = 75\%$). $\cdot-\cdot$, $\ln(\eta z_s/\Delta_y)$; $-\cdot-$, $\ln(\lambda_{3d}/\Delta_y)$; —, $\ln(L_{0.75}/\Delta_y)$. Peak values are indicated as multiples of the cross-stream grid-discretization. Negative values of the logarithms of the grid-normalized dissipation scales are numerical artefacts of the data-analysis algorithms which have been explained in §§ 5.1 and 6.2.2.

physical mechanism that leads to the small-scale intermittency and the corresponding deviation from $Re_\delta^{-3/4}$ scaling may be attributed to the self-stretching component of the strain-rate tensor as introduced in She *et al.* (1990).

Note that the proposed type of $Re_\delta^{-1}$-scaling is determined by the fixed statistics of the rate of spatial-filtering decay, $s$, and hence, it is insensitive to any change in the $\beta_f$ value. On the other hand, the value of the scaling coefficient $\Lambda$ is estimated to be around 3.0 and depends on the chosen value of $\beta_f = 0.75$ in our case.

We can conclude that the spatial filtering technique is capable of capturing most of the local small-scale intermittent behaviour of $\chi$ and the present DNS database supports the estimates in Sreenivasan & Meneveau (1988), Yakhot (2003) and Sreenivasan (2004). The analysis indicates that the resolution requirements for scalar dissipation measurements are much more stringent than the Batchelor scaling would suggest. It also implies that the number of DNS grid points necessary for spatial resolution of the finest (intermittent) structures scales with $N^3 \propto Re^3$, as opposed to the conventionally suggested $N^3 \propto Re^{9/4}$ scaling based on the Kolmogorov scale. The implications for the large-eddy or direct numerical simulations of turbulence due to the stringent scaling constraints imposed by dissipation intermittency have been discussed in detail by Yakhot & Sreenivasan (2005).

## 7. Comparison of the analyses

Differences in the length-scale estimates that originate from the three methods presented above can be best summarized in a comparison of their probability distributions. Figure 13 shows these PDFs of the normalized average and instantaneous dissipation length scales. The one-dimensional cross-stream spectral estimate of the mean dissipation length scale, $\eta_{Z_s}$, has been obtained using (4.2) at all downstream locations along the jet centreline, whereas the instantaneous and local

dissipation length scales, $L_{0.75}$, are computed by spatial filtering of the peak values of the instantaneous cross-stream $\chi$-profiles. Figure 13 also includes the instantaneous normalized three-dimensional dissipation-layer thickness, $\lambda_{3d}$, distribution. All values have been normalized with respect to the minimum grid-discretization, $\Delta_y = 0.0118H$.

Figure 13 shows a very wide distribution of the dissipation length scales represented by $L_{0.75}$ compared to $\eta_{Z_s}$ and $\lambda_{3d}$. It also demonstrates that the bulk of the finest mixing scales present in the flow (owing to the small-scale intermittency of $\chi$) cannot be characterized by the Batchelor scale. The PDF of the instantaneous local dissipation scale, $L_{0.75}$, peaks at a noticeably lower value than that of the spectral dissipation scale estimate, $\eta_{Z_s}$, indicating the necessity for much more stringent resolution requirements than the commonly used scaling with the Batchelor scale. Furthermore, the relatively limited range of dissipation length scales given by $\eta_{Z_s}$ and $\lambda_{3d}$ seems to agree with the limited range of dissipation-layer thicknesses found for direct experimental measurements (Buch & Dahm 1998).

## 8. Conclusions

The DNS database of Pantano (2004) of a turbulent reacting planar jet has been used to estimate the resolution requirements for scalar-dissipation measurements and numerical simulations. It has been shown that the present database is sufficiently resolved in most regions of the flow for studying a highly intermittent variable such as the scalar-dissipation rate. The mean and instantaneous scalar-dissipation length scales were determined by three different methods: spectral analysis, direct investigation of scalar dissipation structures and spatial filtering of the instantaneous mixture fraction field. Scalings and resolution criteria for experiments and simulations based on the easily measurable outer-scale Reynolds number, $Re_\delta$, were then established.

It is shown that the spatial-filtering technique can be used to recover the wide distribution of instantaneous scalar-dissipation length scales that are important in accounting for the small-scale intermittency shown by $\chi$ and these are shown to be proportional to the local-minimum dissipation length scales. This seems to confirm the sufficiency criterion of $\chi$-resolution based on the more stringent $Re_\delta{}^{-1}$ scaling as indicated by the estimates in Sreenivasan & Meneveau (1988), Yakhot (2003) and Sreenivasan (2004) when applied to reactive flows. The study shows that the assumption of exponential decay of intermittent $\chi$ peak-values with increasing filter-width holds. It thus allows the extrapolation to the 'fully resolved' limit and an estimate of the actual resolution needs can be obtained.

The stringent resolution criterion (primarily for DNS studies) suggested in the present study is limited to the resolution of scalar gradients or, equivalently, the scalar dissipation rate, which plays the key role in turbulent scalar mixing. Other physical quantities showing the same (or larger) degree of intermittent behaviour, such as enstrophy, have not been analysed here and the applicability of the suggested resolution criteria to these quantities is beyond the scope of this paper.

The Reynolds-number scaling for the spectrally recovered dissipation length scales is of the Kolmogorov type, while the scaling coefficient, $\Lambda_0$, was estimated to be of order of unity. This implies that the one-dimensional dissipation spectra are able to resolve the true Batchelor scales along the centreline of the evolving jet, without any self-similarity assumptions and at low-to-moderate Reynolds-number values. Notably, computation of instantaneous dissipation-layer thicknesses also yields Batchelor scaling, with similar estimates of the scaling coefficient $\Lambda_{3d}$ that are more conservative than other experimental estimates by Buch & Dahm (1998) and Su &

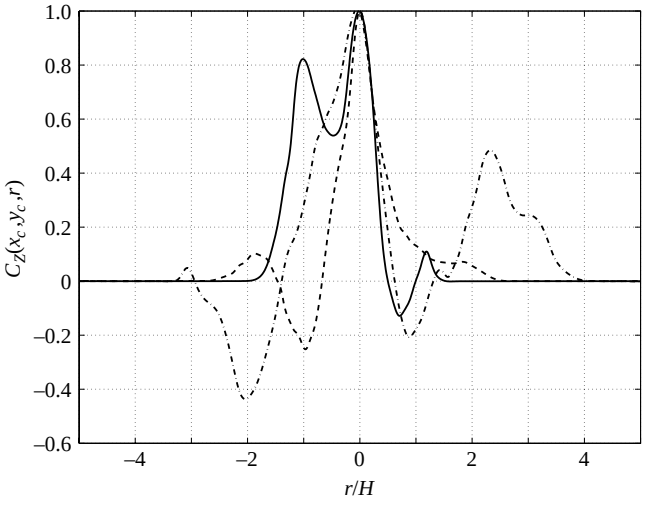


FIGURE 14. Variation of the normalized correlation coefficient $C_Z(x_c, y_c, r)$ with the cross-stream position vector $r$, at various downstream locations along the jet centreline ($y_c/H = 5.0$). All spatial quantities are shown in terms of jet width, $H$. —, $x_c/H = 3.4$; - - -, 8.7;–·–, 13.6. The one-dimensional dissipation spectra corresponding to the correlation coefficients shown are plotted in figure 2.

Clemens (2003) (for reasons explained in § 5.3). However, it is not immediately clear why instantaneous dissipation-layer thicknesses would not yield the $Re_\delta^{-1}$ scaling, evidenced using the spatial-filtering method. A probable explanation may be an inherent averaging involved in the process of computing dissipation contour thicknesses, which yields estimates of the average rather than the true instantaneous dissipation length-scales. Nevertheless, further investigation is required to explain this properly.

The authors would like to thank Robert Barlow (at Sandia) for providing clarifications about the spatial-filtering technique. Financial support by the Engineering and Physical Sciences Research Council via grant GR/T19650 is also gratefully acknowledged. The authors also thank the anonymous reviewers for pointing out some relevant references.

## Appendix A. Computation of one-dimensional dissipation spectra

The two-point cross-stream correlation coefficient at any point $(x_c, y_c)$ along the jet centreline is defined as,

$$R_Z(x_c, y_c, r) = \langle Z'(x_c, y_c, z, t) Z'(x_c, y_c + r, z, t) \rangle, \tag{A 1}$$

where $r$ is the cross-stream distance and subscript $c$ indicates jet centreline values. The average value is computed as a simultaneous mean in temporal ($t$-) and spanwise ($z$-) directions (Pantano 2004), by

$$\langle \phi \rangle(x, y) = \frac{1}{N_T N_z} \sum_{n=1}^{N_T} \sum_{k=1}^{N_z} \phi(x, y, z, t), \tag{A 2}$$

where $N_T$ is the number of time steps and $N_z$ is the number of spanwise planes over which the average of an arbitrary field $\phi(x, y, z, t)$ is computed. Figure 14 shows the

plots of the normalized correlation coefficient,

$$C_Z(x_c, y_c, r) = \frac{R_Z(x_c, y_c, r)}{[\langle Z'(x_c, y_c)^2\rangle \langle Z'(x_c, y_c + r)^2\rangle]^{1/2}}, \tag{A 3}$$

at various downstream locations along the jet centreline. Owing to the complex unstable nature of the studied flow and the small size of the computational domain ($x/H \leqslant 15$), isotropy about the centreplane is not assumed while computing the correlation coefficients, i.e. in general $R_Z(x_c, y_c, r) \neq R_Z(x_c, y_c, -r)$.

The one-dimensional spectrum is defined as

$$E_Z(k_y) = \frac{1}{4\pi} \int_{-\infty}^{\infty} \exp(-\mathrm{i}k_y r) R_Z(r)\, \mathrm{d}r, \tag{A 4}$$

or equivalently by

$$R_Z(r) = 2 \int_{-\infty}^{\infty} \exp(\mathrm{i}k_y r) E_Z(k_y)\, \mathrm{d}k_y, \tag{A 5}$$

where the dependence on $x_c$ and $y_c$ has been dropped for clarity. For homogeneous flow, it is possible to relate $E_Z(k_y)$, using Parseval's identity, to the dissipation spectrum, giving

$$D_Z(k_y) = 2Dk_y^2 E_Z(k_y), \tag{A 6}$$

where we have neglected variation of the molecular diffusion coefficient, $D$, in space owing to changes in temperature.

## Appendix B. Computation of dissipation-layer thicknesses

The algorithm used for identifying the dissipation layers and computing their local thicknesses is shown schematically in figure 15. It essentially deals with a two-dimensional dissipation field in the $(x, y)$-plane. First, the global maximum of the scalar dissipation, $\chi_{max}$, at a specific plane is determined. Secondly, all structures, where $\chi < 0.5\chi_{max}$, are discarded to isolate the regions of strongest dissipative behaviour. A parameter $\beta_m \equiv \chi/\chi_{loc}$ is introduced, which represents the fraction of the local maximum, $\chi_{loc}$, at any point in the scalar dissipation field. The $\beta_m$ parameter demarcates the local spiky topology of the dissipation field for our investigation and values between 50% and 90% are chosen for it. Finally, level sets or iso-contours of the remaining structures at the iso-level of $\beta_m \chi_{loc}$ are determined. It was observed that for the present DNS test case, scalar-dissipation contours at values less than $\beta_m = 0.5$ tend to intersect and thus do not correspond to extreme and isolated dissipative events. This may be an effect of the relatively low-Reynolds-number range in the present DNS, as previous experimental studies of dissipation layers at high Reynolds numbers (Buch & Dahm 1998) do not show this tendency at comparable values of $\beta_m$. However, we are specifically interested in the finest scales of the scalar dissipation and therefore, contours at values below $\chi/\chi_{loc} = 0.5$ are not of direct interest in the present study. On the other hand, the reasoning behind the choice of $\beta_m$ no larger than 0.9 is purely computational. There are too few occurrences for $\beta_m > 0.9$ to obtain reasonably accurate statistics.

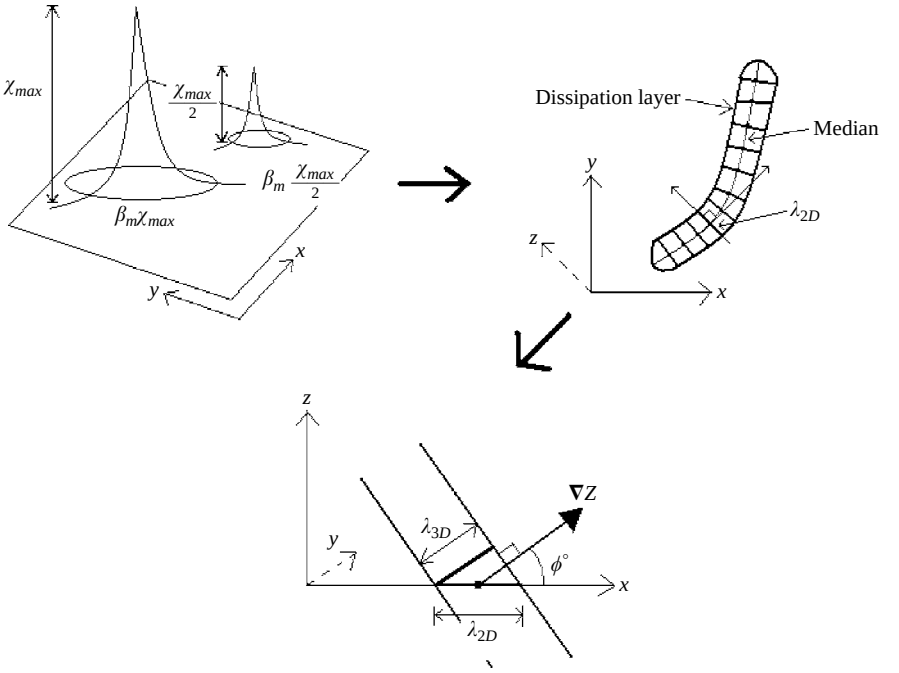


FIGURE 15. Schematic representation of the numerical method employed to investigate the instantaneous scalar-dissipation structures in the three-dimensional computational domain and to compute their thicknesses. Symbols next to the contours indicate the constant values of $\chi$ used to compute the range of contours at a fixed fraction, $\beta_m$, of the local peak values that vary from the global maximum of the planar $\chi$-field, or $\chi_{max}$, to $\chi_{max}/2$.

Once the two-dimensional dissipation layers depicted in figure 15 have been identified, each with its point-to-point connectivity, the algorithm processes the data to compute the median by recognizing the elongated topology of the structure and its corresponding corners. For each point on the contour, the nearest point that is not on its branch between the corners is taken as the fellow-point on the opposite branch. In order to remove computational noise, two points and two corresponding fellow-points are bunched and averaged to obtain a layer midpoint. The line joining these midpoints makes the median for each dissipation layer. Finally, the thickness attributed to each point on the median is computed by calculating the length of the segment orthogonal to the median at that point, whose endpoints manage to be on or just inside the layer boundary in either direction. The measured two-dimensional-layer thickness, $\lambda_{2d}$, at each layer midpoint, is corrected for three-dimensional orientation by the cosine of the out-of-plane angle of the $\nabla Z$ vector (Su & Clemens 2003), to give

$$\lambda_{3d} = \lambda_{2d} \cos\phi. \tag{B 1}$$

This projection becomes less reliable as the dissipation layers align less orthogonally with the plane $(x, y)$ of the flame, i.e. as $\phi$ increases, owing to increasingly significant layer-curvature effects. In similar experimental studies, Su & Clemens (2003), do not consider $\chi$-level sets for which $\phi > 60^\circ$. However, the PDFs of the out-of-plane angle in figure 16 measured at all locations for different values of $\beta_m$ show an extremely high preponderance (around 97%) of $\phi \leqslant 60^\circ$, which makes the correction largely reliable.

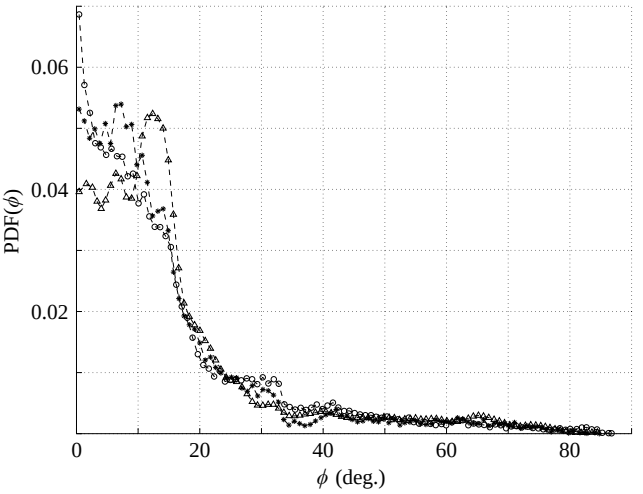


FIGURE 16. PDF of the out-of-plane angle $\phi$ of the scalar-gradient vector for a single computational time step at different $\beta_m$ values. The $\phi$ values have been computed at all dissipation-layer midpoints, for each $\beta_m$ value, at a single computational time step. ○, at $\beta_m = 0.5$; *, 0.75; △, 0.9.

## REFERENCES


BARLOW, R. S. & KARPETIS, A. N. 2005*a* Measurements of scalar variance, scalar dissipation, and length scales in turbulent piloted methane/air jet flames. *Flow Turb. Combust.* **72**, 427–448.

BARLOW, R. S. & KARPETIS, A. N. 2005*b* Scalar length scales and spatial averaging effects in turbulent piloted methane/air jet flames. *Proc. Combust. Inst.* **30**, 673–680.

BATCHELOR, G. K. 1959 Small scale variation of convected quantities like temperature in a turbulent fluid. *J. Fluid Mech.* **5**, 113–133.

BATCHELOR, G. K. & TOWNSEND, A. A. 1949 The nature of turbulent motion at large wave-numbers. *Proc. R. Soc. Lond.* A **199**, 238–255.

BILGER, R. W. 1980 Turbulent flows with nonpremixed reactants. In *Topics in Applied Physics: Turbulent Reacting Flows* (ed. P. A. Libby & F. A. Williams), pp. 65–111. Springer.

BILGER, R. W. 2004 Some aspects of scalar dissipation. *Flow Turb. Combust.* **72**, 93–114.

BILGER, R. W., STÅRNER, S. H. & KEE, R. J. 1990 On reduced mechanisms for methane air combustion in nonpremixed flames. *Combust. Flame* **80** (2), 135–149.

BOERSMA, B. J. 1999 Direct numerical simulation of a turbulent reacting jet. In *Annu. Res. Briefs* CTR, pp. 59–72. Stanford University.

BRETHOUWER, G. & NIEUWSTADT, F. T. M. 2001 DNS of mixing and reaction of two species in a turbulent channel flow: a validation of the conditional moment closure. *Flow Turb. Combust.* **66**, 209–239.

BUCH, K. A. & DAHM, W. J. A. 1996 Experimental study of the fine-scale structure of conserved scalar mixing in turbulent shear flows. Part 1. *J. Fluid Mech.* **317**, 21–71.

BUCH, K. A. & DAHM, W. J. A. 1998 Experimental study of the fine-scale structure of conserved scalar mixing in turbulent shear flows. Part 2. *J. Fluid Mech.* **364**, 1–29.

CORRSIN, S. 1951 On the spectrum of isotropic temperature fluctuations in isotropic turbulence. *J. Appl. Phys.* **22**, 469–473.

DAHM, W. J. A. & SOUTHERLAND, K. B. 1997 Experimental assessment of Taylor's hypothesis and its applicability to dissipation estimates in turbulent flows. *Phys. Fluids* **9** (7), 2101–2107.

DAHM, W. J. A. & SOUTHERLAND, K. B. 1999 Quantitative flow visualization via fully-resolved four-dimensional spatio-temporal imaging. In *Flow Visualization: Techniques and Examples* (ed. A. Smits & T. T. Lim), pp. 231–258. Imperial College Press, London.

DAHM, W. J. A., SOUTHERLAND, K. B. & BUCH, K. A. 1991 Direct, high resolution, four-dimensional measurements of the fine scale structure of $Sc \gg 1$ molecular mixing in turbulent flows. *Phys. Fluids* A **3** (5), 1115–1127.

Donzis, D. A., Sreenivasan, K. R. & Yeung, P. K. 2005 Scalar dissipation rate and dissipative anomaly in isotropic turbulence. *J. Fluid Mech.* **532**, 199–216.

Frisch, U. 1991 From global scaling, *a la* Kolmogorov, to local multifractal scaling in fully developed turbulence. *Proc. R. Soc. Lond.* A **434**, 89–99.

Frisch, U. 1995 *Turbulence: The Legacy of A. N. Kolmogorov*. Cambridge University Press.

Frisch, U. & Vergassola, M. 1991 A prediction of the multifractal model: the intermediate dissipation range. *Europhys. Lett.* **14**, 439–444.

Gibson, C. H. 1991 Kolmogorov similarity hypotheses for scalar fields: sampling intermittent turbulent mixing in the ocean and galaxy. *Proc. R. Soc. Lond.* A **434**, 149–164.

Grant, H. L., Stewart, R. W. & Moilliet, A. 1962 Turbulent spectra from a tidal channel. *J. Fluid Mech.* **12**, 241–268.

Kolmogorov, A. N. 1941 The local structure of turbulence in incompressible viscous fluid for very large Reynolds numbers. In *C. R. Dokl. Akad. Sci. URSS*, **30**, 301–305.

Kolmogorov, A. N. 1962 A refinement of previous hypotheses concerning the local structure of turbulence in a viscous incompressible fluid at high Reynolds numbers. *J. Fluid Mech.* **13**, 82–85.

Kushnir, D., Galun, M. & Brandt, A. 2006*a* Fast multi-scale clustering and manifold identification. *Pattern Recog.* **39**, 1876–1891.

Kushnir, D., Schumacher, J. & Brandt, A. 2006*b* Geometry of intensive scalar dissipation events in turbulence. *Phys. Rev. Lett.* **97** (124502), 1–4.

Lele, S. K. 1992 Compact finite difference schemes with spectral-like resolution. *J. Comput. Phys.* **103**, 16–42.

Mathieu, J. & Scott, J. 2000 *An Introduction to Turbulent Flow*. Cambridge University Press.

Meneveau, C. & Sreenivasan, K. R. 1991 The multifractal nature of turbulent energy dissipation. *J. Fluid Mech.* **224**, 429–484.

Mizobuchi, Y., Shinjo, J., Ogawa, S. & Takeno, T. 2005 A numerical study on the formation of diffusion flame islands in a turbulent hydrogen jet lifted flame. *Proc. Combust. Inst.* **30**, 611–619.

Monin, A. S. & Yaglom, A. M. 1971 *Statistical Fluid Mechanics; Mechanics of Turbulence*, 1st edn. MIT Press.

Nelkin, M. 1994 Universality and scaling in fully developed turbulence. *Adv. Phys.* **43**, 143–181.

Noullez, A., Wallace, G., Lempert, W., Miles, R. B. & Frisch, U. 1997 Transverse velocity increments in turbulent flow using the RELIEF technique. *J. Fluid Mech.* **339**, 287–307.

Oboukhov, A. M. 1949 Struktura temperaturnovo polia v turbulentnom potoke. *Izv. Akad. Nauk SSSR Geofiz.* **3**, 59.

Pantano, C. 2004 Direct simulation of non-premixed flame extinction in a methane–air jet with reduced chemistry. *J. Fluid Mech.* **514**, 231–270.

Peters, N. 2000 *Turbulent Combustion*. Cambridge University Press.

Pitts, W. M., Richards, C. D. & Levenson, M. S. 1999 Large- and scall-scale structures and their interactions in an axisymmetric jet. *Tech. Rep.* 6393. NIST.

Pope, S. 2000 *Turbulent Flows*, pp. 222–237. Cambridge University Press.

Saddoughi, S. G. & Veeravalli, S. V. 1994 Local isotropy in turbulent boundary layers at high Reynolds numbers. *J. Fluid Mech.* **268**, 333–372.

Schumacher, J., Sreenivasan, K. R. & Yeung, P. K. 2005 Very fine structures in scalar mixing. *J. Fluid Mech.* **531**, 113–122.

She, Z.-S. 1991 Physical model of intermittency in turbulence: near-dissipation-range non-Gaussian statistics. *Phys. Rev. Lett.* **66**, 600–603.

She, Z.-S., Jackson, E. & Orszag, S. A. 1990 Intermittent vortex structures in homogeneous isotropic turbulence. *Nature* **344**, 226–228.

She, Z.-S., Chen, S., Doolen, G., Kraichnan, R. H. & Orszag, S. A. 1993 Reynolds number dependence of isotropic Navier–Stokes turbulence. *Phys. Rev. Lett.* **70**, 3251–3254.

Sreenivasan, K. R. 1991 Fractals and multifractals in fluid turbulence. *Annu. Rev. Fluid Mech.* **23**, 539–600.

Sreenivasan, K. R. 2004 Possible effects of small-scale intermittency in turbulent reacting flows. *Flow Turb. Combust.* **72**, 115–131.

Sreenivasan, K. R. & Antonia, R. A. 1997 The phenomenology of small-scale turbulence. *Annu. Rev. Fluid Mech.* **29**, 435–472.

Sreenivasan, K. R. & Meneveau, C. 1988 Singularities of the equations of fluid motion. *Phys. Rev.* A **38**, 6287–6295.

Sreenivasan, K. R. & Stolovitzky, G. 1996 Statistical dependence of inertial range properties on large scales in high-Reynolds-number shear flow. *Phys. Rev. Lett.* **77**, 2218–2221.

Su, L. K. 1998 Measurements of the three-dimensional scalar dissipation rate in gas-phase planar turbulent jets. In *Annu. Res. Briefs* CTR, pp. 35–46. Stanford University.

Su, L. K. & Clemens, N. T. 2003 The structure of fine-scale scalar mixing in gas-phase planar turbulent jets. *J. Fluid Mech.* **488**, 1–29.

Tennekes, H. & Lumley, J. L. 1974 *A First Course in Turbulence*. MIT Press.

Tsurikov, M. S. & Clemens, N. T. 2002 The structure of dissipative scales in axisymmetric turbulent gas-phase jets. *AIAA J.* **0164**, 1–16.

Vedula, P., Yeung, P. K. & Fox, R. O. 2001 Dynamics of scalar dissipation in isotropic turbulence: a numerical and modelling study. *J. Fluid Mech.* **433**, 29–60.

Wang, G.-H., Barlow, R. S. & Clemens, N. T. 2007*a* Quantification of resolution and noise effects on thermal dissipation measurements in turbulent non-premixed jet flames. *Proc. Combust. Inst.* **31**, 1525–1532.

Wang, G.-H., Karpetis, A. N. & Barlow, R. S. 2007*b* Dissipation length scales in turbulent nonpremixed jet flames. *Combust. Flame* **148**, 62–75.

Wang, L. & Peters, N. 2006 The length-scale distribution function of the distance between extremal points in passive scalar turbulence. *J. Fluid Mech.* **554**, 457–475.

Wang, L.-P., Chen, S. & Brasseur, J. G. 1999 Examination of hypotheses in the Kolmogorov refined turbulence theory through high-resolution simulations. Part 2. Passive scalar field. *J. Fluid Mech.* **400**, 163–197.

Williams, F. A. 1985 *Combustion Theory*, 2nd edn. Addison–Wesley.

Yakhot, V. 2003 Pressure–velocity correlations and scaling exponents in turbulence. *J. Fluid Mech.* **495**, 135–143.

Yakhot, V. & Sreenivasan, K. R. 2005 Anomalous scaling of structure functions and dynamic constraints on turbulence simulations. *J. Stat. Phys.* **121**, 823–841.

Yeung, P. K., Xu, S., Donzis, D. A. & Sreenivasan, K. R. 2004 Simulations of three-dimensional turbulent mixing for Schmidt numbers of the order 1000. *Flow Turb. Combust.* **72**, 333–347.

Yeung, P. K., Donzis, D. A. & Sreenivasan, K. R. 2005 High-Reynolds-number simulation of turbulent mixing. *Phys. Fluids* **17**, 081703.